A. ISHLINSKY INSTITUTE FOR PROBLEMS IN MECHANICS
RUSSIAN ACADEMY OF SCIENCES

Schlumberger

A.V. BAZILEVSKY[1], V.A. KALINICHENKO[1],
V.A. PLYASHKEVICH[2], D.V. BADAZHKOV[2], A.N. ROZHKOV[1]

[1] *A. Ishlinsky Institute for Problems in Mechanics, Russian Academy of Sciences, Moscow, 119526, Russia*

[2] *Schlumberger Technology Corporation, Novosibirsk, 630060, Russia*

SEDIMENTATION OF PARTICLES IN SHEAR FLOWS OF VISCOELASTIC FLUIDS WITH FIBERS

Preprint № 1127

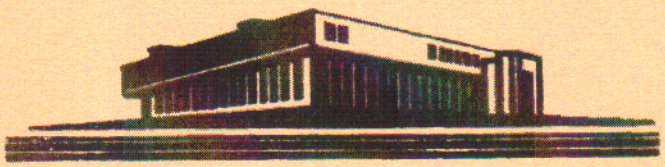

Moscow 2016

A. ISHLINSKY INSTITUTE FOR PROBLEMS IN MECHANICS
RUSSIAN ACADEMY OF SCIENCES

A.V. BAZILEVSKY[1], V.A. KALINICHENKO[1],
V.A. PLYASHKEVICH[2], D.V. BADAZHKOV[2], A.N. ROZHKOV[1]

[1] *A. Ishlinsky Institute for Problems in Mechanics, Russian Academy of Sciences, Moscow, 119526, Russia*

[2] *Schlumberger Technology Corporation, Novosibirsk, 630060, Russia*

SEDIMENTATION OF PARTICLES IN SHEAR FLOWS OF VISCOELASTIC FLUIDS WITH FIBERS

Preprint № 1127

Moscow 2016

ABSTRACT

The preprint presents the effects of fiber additives on rheology and sedimentation of particle suspension in viscoelastic basic fluid when the suspension is subjected to shear flow. It was demonstrated experimentally that fiber additives (millimeters long and micrometers diameter at hundredth mass fraction) increase viscosity and retard sedimentation significantly. At the same mass concentration, long and thin fibers reduce sedimentation rate and increase suspension viscosity larger than short and thick fibers. It was shown that both rheology and sedimentation are controlled by single conformational parameter which is the product of the fiber number density and cube of fiber length (overlap parameter).

АННОТАЦИЯ

Препринт представляет эффекты добавок волокон на реологию и седиментацию суспензии твёрдых частиц в вязкоупругой базовой жидкости в условиях сдвигового течения. Экспериментально показано, что добавки волокон (миллиметровой длины и микронного диаметра при массовой доле менее одного процента) значительно увеличивают вязкость и замедляют седиментацию. При одинаковой массовой доле длинные и тонкие волокна снижают скорость седиментации и увеличивают вязкость суспензии больше, чем короткие и толстые волокна. Было показано, что реология и седиментация управляются единым конформационным параметром, который является произведением числа волокон в единице объёма и куба контурной длины волокна.

ISBN 978-5-91741-174-3
055(02)2 ©

Introduction

The gravity-induced sedimentation of particles in a complex fluid is an important element of hydraulic fracturing (HF) technology in the oil and gas industry. HF fluid is the dense suspension which consists on some basic fluid (viscous or viscoelastic) and solid particles. HF fluid under high pressure forms the fracture, fills it by solid particles which prevents the fracture close just after pressure remove. During the flow of HF fluid in the fracture the particles are subjected to sedimentation which causes particle losses. The suppression of particle losses is main feature of HF fluid. For example, the simplest way to reduce the particle losses is to increase the effective fluid viscosity. On the other hand, the rheological properties of the hydraulic fracturing fluid must provide easy flow in the fracture. Therefore, the set of properties of the hydraulic fracturing fluid is the compromise between particle transport capability of the fluid and its appropriate hydrodynamics in the fracture.

Limited number of studies is dedicated to study the particle transport properties of the viscous and viscoelastic fluids. The experiments with Couette flow of viscoelastic fluids with particles demonstrated that the sedimentation of a single particle and concentrated suspensions in viscoelastic fluids typically is accelerated with an increase in the shear rate (Gheissary and van der Brule 1996, Liu and Sharma 2005, Roodhart 1985, Bazilevskii et al. 2010). Acceleration of sedimentation under action of external shear flow occurs also in Newtonian fluid if sedimentation happens near plane wall (Bazilevskii and Rozhkov 2009). Dogon and Golombok (2016) demonstrated different sedimentation modes in shear thickening viscoelastic surfactant fluids.

An addition of a small amount of thin flexible fibers into the hydraulic fracturing fluid can modify rheological and sedimentation properties of the

fluid noticeably. The rheology of the fiber suspensions is different from the rheology of all other solid-liquid systems that is taken into account in the pulp and paper industry (Petrie 1999, Ventura et al. 2007). As for sedimentation, it was shown by Elgaddafi et al. (2012) that the sedimentation of a single 2–8 mm particle in a quiescent viscous or viscoelastic fluid can be reduced significantly (up to complete cessation) by means of fibers with 10 mm length and 100 μm diameter at 0–0.08% weights concentration. At the same time, the influence of fibers on viscosity was not observed.

Another set of suspension parameters was investigated in the study by Bazilevsky et al. (2016). The particles of 0.66 mm diameter at 0-30% volume concentration and fibers of 6 mm length, 12 μm at 0–0.4% mass fraction were studied. Only Newtonian fluid (glycerol) was used as the basic fluid. The sedimentation was studied not only in quiescent suspension but also in the case when the fluid is subject to shear flow in the horizontal plane. In the fiber-free particle-laden suspension, the viscosity and particle sedimentation velocity are not dependent on the shear rate. Experiments with fiber additives revealed a significant increase in the viscosity and a decrease in particle sedimentation rate in quiescent suspension and suspensions under low shear flow. Effect of fibers becomes more pronounced with an increase in the fiber concentration. At the same time, the fibers do not change rheology and sedimentation appreciably at high shear rates $\dot{\gamma}$~100 s^{-1}. Thus the viscosity of the fiber-particle suspension in glycerol decreases and the particle sedimentation velocity increases as the shear rate increases. Analysis of the experimental data shows that, as the first approximation, the sedimentation velocity can be described by the universal function, which is inversely proportional to the actual viscosity of the suspension.

The present work was undertaken to study the rheology and sedimentation of particle suspensions in fiber-laden fluid under shear flow

when viscoelastic fluid is used as the basic fluid. Moreover the effects of fiber length and diameter on rheology and particle sedimentation in viscoelastic basic fluid were studied also.

1. Visualization of particles sedimentation in suspension of fibers with different geometries

1.1. Statement of problem. The purpose of this section was to apply the developed method of experimental investigation of the particle (P) sedimentation in the shear flows (Bazilevsky et al. 2016) for study this phenomenon in the viscoelastic basic fluid.

1.2. Materials and method. The guar gum solution (GG-0.48%) was used as basic viscoelastic fluids. It was prepared by adding a of 2.4 g of guar powder to distilled water of 500 ml volume being in the cap of the working blender; the blender speed is 1200-1500 rpm. At this speed value a funnel arose at the center of the cap but foaming was still absent. The time of stirring was 30 min. After that, aging of the solution without mixing during about 30 min followed to complete its gelling and air bubbles leaving.

In the experiments the Poly Lactic Acid (PLA) polymer fibers, density 1200 kg/m^3, geometry (length/diameter) 6mm/12μm, 3mm/12μm, 6mm/8μm, crimped shape – were used as tested fibers (Shalagina and Fu 2015, Shalagina et al. 2015).

Microphotographs of the fibers are shown in Fig. 1. The fibers were supplied by Schlumberger as a number of fiber bundles. Before suspension preparation fiber bundles were dispersed and fluffed by means of the procedure used previously (Bazilevsky et al. 2016). According to this procedure, the amount of the fibers with a weight of 0.5-1 g was fluffed in a coffee grinder SINBO SCM 2929 for 3-5 sec sequentially three times. The required amount of the fluff fibers was added to 60 g of guar gum aqueous

solution GG-0.48% and stirred manually or in a magnetic stirrer. Weighting of the fibers by electronic balances OHAUS AR3130 with an accuracy of 0.001 g was used.

The ceramic particles (fraction 20/40) with an average diameter of d_p=0.66 mm (standard deviation 0.07 mm) and density of 2710 kg/m^3 were used as solid phase.

In the experiments we varied the weight concentration of the fibers F = 0, 0.1, 0.24, 0.4%, and the volume concentration of particle P = 0, 20, 24, 30%.

The experimental method consists in the observation of sedimentation of particles in a gap between two cylindrical surfaces (Fig. 2). The gap was created by the coaxial configuration of two cylinders (outer and inner). The outer cylinder was a transparent tube, which made it possible to observe the processes occurred in the gap. To create a shear flow in the gap (the Couette flow), the inner cylinder was rotated at a fixed frequency f . The combinations of the geometrical and kinematic parameters of the set-up used in the experiments are given in Table 1. The table also contains the information about the ratio of cylinders radii k=R_0/R_i and the range of shear rates realized in the flow.

Table 1

Configuration	$2R_i$, mm	$2R_o$, mm	$R_o - R_i$, mm	$k = R_o / R_i$	H, mm	$\dot{\gamma}$, s^{-1}
S3	32.0	43.9	5.95	1.372	72.0	0 - 108.6

The gap between the cylinders was filled with GG solution or with a homogeneous suspension for studying for viscosity measurements and studies of suspensions' sedimentation.

The shear rate $\dot{\gamma}$ in the gap was determined by the cylinder radii R_0 and R_i and the rotation frequency of inner cylinder f:

$$\dot{\gamma} \cong 2\pi f/(k\text{-}1)\times 2k^2/(k+1) \qquad (1.1)$$

Table 2 shows the shear rate used in the present study. The first line represents the gear numbers of a viscometer. The second line represents the frequency of rotation of the inner cylinder $f = \omega / 2\pi$. The third line contains the values of the shear rates.

Table 2

Gear#	4a	6a	8a	10a	11a	12a
f, rpm	3	9	27	81	135	243
$\dot{\gamma}$, s^{-1}	1.340	4.021	12.065	36.197	60.329	108.593

The shear stress at the inner cylinder is given by $\tau = M / (2\pi R_i^2 H_1)$, where M is the viscous friction torque on the internal surface of the inner cylinder, H_1 is the immersed length of the inner cylinder. The torque M is determined by the winding angle of a special spring (a dynamometer). The shear viscosity of the suspension is defined as $\mu=\tau/\dot{\gamma}$.

Measurements were performed as follows - Fig. 3. The required quantity of a particles of the initial volume concentration P=0, 20, 24 or 30% was added to a suspension of a predetermined concentration of fibers F=0, 0.1, 0.24 or 0.4%. For given fiber concentration F all tests with particle concentrations P=0, 20, 24 or 30% were conducted with the same GG solution. We consequently added particles into the suspension sample to go to the next particle concentration. However each next fiber concentration F=0, 0.1, 0.24 or 0.4% was studied with fresh GG solution.

The tested suspension (75-85 ml) was mixed in a glass measuring beaker using a magnetic stirrer and/or manually (Fig. 3a). When the suspension took the homogeneous view the beaker was quickly (for 2-3 s) elevated to immerse the inner (rotating at a given speed) cylinder into the fluid. At a time a special table of a preset height was set under the bottom of

the beaker to fix the immersion depth H_1=36 mm, forming the metering geometry (Fig. 3b). Just after that reading of the multimeter was followed, and the digital signal proportional to the torque M was saved to a computer.

The motion of a sedimentation front was simultaneously recorded by a digital camera. After that cylinder's speed of rotation was stepwise changed, the above steps were repeated again to obtain the dependence of the signal on the speed. Using the dependence and the corresponding relations, the flow curves of the suspension, $\tau(\dot{\gamma})$ and $\mu(\dot{\gamma})$, were calculated.

All the measurements were carried out at a room temperature of 21-23 ^{0}C. It is likely that at more high temperature the suspension viscosity will decrease that will cause acceleration of the sedimentation processes (Barnes et al. 1989).

1.3. Determination of front position and sedimentation velocity. For registration of the sedimentation front, we used the digital video camera DIMAGE Z2 (frame rate of 15 fps, F/2.8-3.6). Post-processing of video frames was carried out by ImageJ 1.46b software. Image resolution was 0.16 mm/pixel or 6.28 pixels/mm. On the frames the areas with a higher concentration of the dispersed phase appeared darker, and ones with less particles were light - Fig. 4a. Thus, an optical density of the image, which characterizes the attenuation of light, can be used as a measure of transparency of the analyzed suspension for light rays. The optical density depends primarily on the density of the suspension (or particle concentration), through which the light beam passes.

To construct a vertical profile of relative concentration in the form of the vertical dependence of the intensity $I(y)$ along a vertical line we used the software ImageJ 1.43u. To average the local variations in the intensity $I(y)$ in the horizontal direction we used a vertical line width of 100 pixels or 20 mm, which corresponds to about 30 diameters of the particle particles - Fig. 4b.

The corresponding vertical profiles of the pixels intensity are shown in Fig. 4c. The phase of pure liquid is characterized by a maximum intensity $I_{\max}$, and phase of the suspension by a minimum intensity $I_{\min}$. Between these two areas there is a transition region of finite thickness. Consequently, the position of the sediment front h can be determined by the value h, corresponding to half the sum of the minimum and maximum pixel intensities $I(h)= (I_{\max} + I_{\min}) / 2$.

We used the function $h(t)=h_0+v_s t$ to approximate the position $h(t)$ of the sedimentation front in experiments. The parameter v_s corresponds to the front velocity, time t runs from the moment of termination of the mixing process.

As an example, data on the front sedimentation of particle of initial volume concentration P=24% in guar gum GG-0.48% with additives of tested fibers 3mm/12μm in shear flow 11a, $\dot{\gamma}$=60.32 s^{-1} are shown in Fig. 5. The corresponding value of the sedimentation velocity is v_s=0.447 mm/s. The described method of determining the sedimentation velocity was used in the processing of all experimental data on the particle sedimentation (P= 20, 24, 30%) in pure base liquid (F=0), and in base liquid with fibers (F= 0.1, 0.24, 0.4%).

Note that at high shear rates the sedimentation front is unstable - it is blurring. This leads to severe irregularity of the relative concentration profile in the form of vertical depending of the intensity $I(y)$. In the issue, it is difficult to estimate the sedimentation velocity v_s. Since the value of the estimated velocity v_s in this case depends essentially on the choice of the processed video frames and of the position of the control line along which the relative concentration profiles are constructed, in the summary table (see below) we give several values of the velocity of sedimentation.

1.4. Determination of settling velocity of a single particle. The settling velocity v_s of a single particle in base and composite (with fibers)

fluids was estimated as follows.

From video material on deposition process we selected video frames, which describe the vertical displacement of the particle, and the dependence $h(t)$ was plotted. Then the approximation function $h(t)=h_0+v_s t$ was used, and the value v_s was determined.

As an example, Fig. 6 includes data on the sedimentation of a single particle in guar gum GG-0.48% with additives of fibers 3mm/12μm and 6mm/12μm at F=0.1%; regimes of Still (quiescent) $\dot{\gamma}=0$ s^{-1} and 12a $\dot{\gamma}=108.6$ s^{-1}. The corresponding values of the sedimentation velocity were estimated as v_s= 0.308 and 1.681 mm/s.

Note that during mixing it is impossible to achieve a completely uniform distribution of fiber in base liquid (guar gum). For this reason the deposition of a single particle to a large extent depends on the initial location of the particle. We can assume that when a single particle hits in a fiber tangle, it almost does not settle for times up to two minutes and has zero or close to zero velocity v_s. On the other hand, the particle may enter between the fiber clusters - in this case its settling velocity is high. In view of the foregoing, the summary table shows several values of the settling velocity of a single particle.

At the end of this section we note that the particle diameter d_p=0.66 mm and contour length of fiber l=3 or 6 mm are not too small compared with the gap aperture between two cylindrical surfaces R_0-R_i=5.95 mm. The equal order of the particle/fiber dimension and flow dimension can disturb linear velocity profile along the gap and therefore can complicate the measurement interpretation (Barnes et al. 1989). However our previous research (Bazilevskii et al. 2010) approves certainly that successive transition from a 6-mm annulus to a 10 and 36-mm annulus does not cause remarkable changes in the data for the suspension of 0.66 mm particles. We suppose that the

effect of fibers on the velocity profile is also negligible because of absence of visible stratification of fiber suspension along the gap.

2. Results of rheological and sedimentation measurements in the shear flow

2.1. Viscometric data. The data of viscometric and sedimentation tests of suspensions of fiber (F) and ceramic particles (P) in Guar Gum (GG) are shown in Fig. 7. In particular the plots show the dependences of shear stress τ and shear viscosity $\mu=\tau/\dot{\gamma}$ versus shear rate $\dot{\gamma}$.

Comparison of the plot for F=0 with that of F=0.1, 0.24 and 0.4% shows that the most significant effect of fibers on suspension rheology results in high increase of shear stress at low shear rates $\dot{\gamma}\sim1$ s^{-1} as well as at high shear rates $\dot{\gamma}\sim100$ s^{-1}. Addition of only 0.4% fibers gives the 10-fold increase in the shear viscosity at shear rate $\dot{\gamma}=1$ s^{-1}, whereas the Einstein formula predicts growth only in 1.01 times. The stress (and viscosity) increases with the fiber and particle concentrations.

Plots show that fiber geometry influences significantly on the rheology of fiber-particle suspension. The most significant increase in the shear stress was provided by the long and thin fibers 6mm/8μm, but short and thick fibers 3mm/12μm gave a minimum effect on the shear stress. Thus one can conclude that at given mass concentration of fibers F the shear stress τ (as well as viscosity μ) increases with the increasing of fiber length l and decreasing of fiber diameter d_f.

The flow curves $\tau(\dot{\gamma})$ in Fig. 7 are approximately linear for all tested liquids. Therefore the shear rheology of fiber-particle suspensions can be modeled by the power law model

$$\tau=K\dot{\gamma}^n \qquad (2.1)$$

where τ is the shear stress, K is the consistency, n is the flow index. Parameters K and n were determined by means of fitting the experimental curves with formula (2.1) as it is demonstrated by plots $\tau(\dot{\gamma})$ and $\mu(\dot{\gamma})$ in Fig. 7. The fitting was conducted by means of least squares method using the graphics software package Origin 6.1. The calculations were performed in the mode 'No weighting'. Results of fitting procedure are shown in Table 3 as well as in Fig. 8.

Table 3 Viscometric data of the tested liquids

***F*=0**

Fiber	*F*, mass%	*P*, vol%	*K*	*n*
No	0	0	0.66883+-0.09834	0.59607+-0.03499
No	0	20	0.77557+-0.09521	0.62429+-0.0283
No	0	24	0.83383+-0.04731	0.62847+-0.01307
No	0	30	1.39682+-0.17811	0.56037+-0.02973

***F*=0.1%**

Fiber	*F*, mass%	*P*, vol%	*K*	*n*
No	0	0	0.77499±0.08205	0.5703±0.0254
6mm/12μm	0.1	0	1.60413+-0.11523	0.44771+-0.01799
	0.1	20	2.64513+-0.36593	0.393+-0.03361
	0.1	24	2.95038+-0.31828	0.40283+-0.02613
	0.1	30	3.73002+-0.30976	0.40299+-0.02011
3mm/12μm	0.1	0	0.77404+-0.0846	0.57573+-0.02618
	0.1	20	1.35634+-0.21617	0.50932+-0.03755
	0.1	24	1.97412+-0.11424	0.45419+-0.01381
	0.1	30	2.44652+-0.19666	0.45375+-0.01919
6mm/8μm	0.1	0	3.14279+-0.13822	0.33187+-0.01171
	0.1	20	3.94651+-0.33429	0.33239+-0.02102
	0.1	24	4.56053+-0.23176	0.34162+-0.01257
	0.1	30	5.97872+-0.42827	0.32487+-0.01783

***F*=0.24%**

Fiber	*F*, mass%	*P*, vol%	*K*	*n*
No	0	0	0.6032+-0.05755	0.6233+-0.02257
6mm/12μm	0.24	0	3.66155+-0.17197	0.31694+-0.01262
	0.24	20	5.39533+-0.33351	0.30454+-0.01551
	0.24	24	6.11746+-0.43735	0.29908+-0.01799
	0.24	30	7.40147+-0.5701	0.30048+-0.01937
3mm/12μm	0.24	0	1.46384+-0.0892	0.47929+-0.01507
	0.24	20	2.67817+-0.21856	0.42638+-0.01963

	0.24	24	3.5277+-0.5095	0.39395+-0.03508
	0.24	30	4.97637+-0.60054	0.34529+-0.0298
6mm/8μm	0.24	0	7.1569+-0.40499	0.25944+-0.01589
	0.24	20	9.52598+-0.65836	0.23184+-0.01797
	0.24	24	10.23076+-1.08782	0.26097+-0.02723
	0.24	30	12.11454+-0.74173	0.25978+-0.01569

***F*=0.4%**

Fiber	*F*, mass%	*P*, vol%	*K*	*n*
No	0	0	0.50515+-0.11227	0.64241+-0.05226
6mm/12μm	0.4	0	4.93765+-0.22746	0.29946+-0.01253
	0.4	20	6.80205+-0.60485	0.28688+-0.02249
	0.4	24	8.06577+-0.63736	0.27153+-0.02013
	0.4	30	8.8105+-0.56326	0.28552+-0.01618
3mm/12μm	0.4	0	2.04931+-0.13373	0.41932+-0.01655
	0.4	20	3.47325+-0.27361	0.3775+-0.01923
	0.4	24	4.22978+-0.26334	0.3651+-0.01527
	0.4	30	4.77608+-0.31877	0.36494+-0.01637
6mm/8μm	0.4	0	10.36166+-0.40786	0.21358+-0.01152
	0.4	20	11.40662+-1.11557	0.2597+-0.02506
	0.4	24	11.8947+-0.73571	0.26632+-0.0158
	0.4	30	13.88809+-1.25434	0.24641+-0.0233

The results show that the rheological behavior of GG-based suspensions with the addition of fibers is essentially non-Newtonian. In all cases the flow index *n* is markedly less than unity. Thus the fiber-containing suspensions in GG can be characterized as shear-thinning liquids.

There is the strong influence of fibers concentration *F* and particles concentration *P* on the consistency *K*. Consistency *K* increases in several times with increasing *P* and *F*. A combined influence of factors *P* and *F* leads to the multiplier effect of *P* and *F*, when the resulting value of *K* (for maximum concentrations *F*=0.4%, *P*=30%) is significantly greater than all other values of *K*. In the studied range of parameters the flow index *n* decreases with increasing *F* and does not vary noticeably with growth of *P*.

Effect of fiber geometry on rheological parameters is noticeable. At given mass concentration of fibers F and volume particle concentration P the consistency K increases markedly with the growth of fiber length l and decreasing of fiber diameter d_f. Inverse effect is observed for flow index n.

Observed high growth of inner stresses in fiber containing suspension validates assumption that deformation of fiber network in the liquid is dominant process which forms the inner stresses in the suspension. Estimates show that fibers in suspensions studied are subjected to high overlap. The measure of overlap is average volume fraction (overlap parameter) cl^3, where c is the number of fibers per unit volume and l is the contour fiber length [Hinch 1977, Harlen et al. 1999]. Roughly speaking the fibers overlap if $cl^3>1$ and such suspensions are supposed to be concentrated. Fibers do not contact with each other if $cl^3<1$ and such suspensions are supposed to be diluted. The parameter cl^3 equals $F(4/\pi)\ (\rho_{GG}/\rho_f)\cdot(l/d_f)^2$, where ρ_{GG} is the density of Guar gum. Taking ρ_{GG}=1000 kg/m^3, ρ_f =1200 kg/m^3 we obtain that cl^3 comes out as it is shown Table 4. All these magnitudes mean that the fibers overlap and suspensions under investigations can be characterized as concentrated.

Table 4 Overlap parameter cl^3 in fiber suspensions under investigation

	F			
Fiber	0%	0.1%	0.24%	0.4%
6mm/12μm	0	265	637	1061
3mm/12μm	0	66	159	265
6mm/8μm	0	596	1432	2387

In concentrated fiber suspension the efficiency of fiber network on deformation resistance is defined by overlap and possible entanglement of the fibers in the network. The fiber thickness in given network structure does not influence on the resistance because 1) friction between fibers does not depend on fiber diameter and 2) hydrodynamical counteraction of a fiber with a solvent is defined by the fiber length and weak dependence versus fiber

diameter d_f [Hinch 1977]. If that so we can suggest that fiber suspension rheology depends on number of fibers per unit c, fiber length l and do not depend on fiber diameter d_f. According to π-theorem the solely dimensionless combination of these constitutive variables is combination cl^3.

To check this hypothesis the dependences of shear stress τ versus fiber mass concentration F and versus overlap parameter cl^3 are constructed in Fig. 9. The plots were obtained for all studied fibers (6mm/12μm, 3mm/12μm, 6mm/8μm,), for shear rates $\dot{\gamma}_{\dot{\gamma}}$=1.34, 4.02, 12.06, 36.19, 60.32, 108.5 s^{-1} and particles volume concentrations P=0 and 24%.

Data show that for given mass concentration F (left graphs) long and thin fibers 6mm/8μm increase shear stress larger than other fibers. Fibers 6mm/12μm give intermediate stress growth. Effect of short and thick fiber 3mm/12μm is less than effects of the two other fibers types.

At the same time for given overlap parameter cl^3 all the fibers provide approximately the same shear stress τ (right graphs): for given shear rate $\dot{\gamma}_{\dot{\gamma}}$ and particle concentration P all points of shear stress are accumulated along a single universal curve if dependencies versus overlap parameter cl^3 are considered. Each of these dependences is fitted well by the single linear curve as shown on the plots in Fig. 9.

The rheological parameters K and n were also re-plotted as functions of overlap parameter cl^3 - Fig. 8, right graphs. All experimental points are located on a single universal surface which depends only on overlap parameter cl^3 and particle concentration P.

Thus, observations validate the statement that the rheology of fiber-particle suspensions is defined by overlap parameter cl^3. In particular, unlike fiber length l, the fiber diameter d_f does not influence on rheology of fiber suspension if the number of particles in the volume unit c is fixed.

2.2. Sedimentation data. Table 5 presents the summary of data on the particles sedimentation in guar gum with the addition of fibers PLA2mod of three types: 6mm/12μm, 3mm/12μm and 6mm/8μm. The sedimentation velocity v_s of single particles and the sedimentation velocity of the suspension of particles at various concentrations of particles P and fibers F are shown.

Table 5 Particle sedimentation velocities: single particles and suspensions

***F*=0**

Fiber	*F*, %	*P*, %	v_s, mm/s						
			Quiescent $\dot{\gamma}=0$	4a 1.34 s^{-1}	6a 4.02 s^{-1}	8a 12.06 s^{-1}	10a 36.19 s^{-1}	11a 60.32 s^{-1}	12a 108.5 s^{-1}
No	0	0(single)	1.565	1.058	1.994	2.229 2.555	2.251 2.453	1.901	2.536
No	0	20	0.965	0.905	0.900	0.857 0.904	1.318	2.088	2.381
No	0	24	0.816	0.548	0.604	0.708 0.740	1.146	1.501 1.849	1.740 2.106
No	0	30	0.529 0.798	0.379	0.372	0.432	0.625	0.846 1.011	0.876 1.098

***F*=0.1%**

Fiber	*F*, %	*P*, %	v_s, mm/s						
			Quiescent $\dot{\gamma}=0$	4a 1.34 s^{-1}	6a 4.02 s^{-1}	8a 12.06 s^{-1}	10a 36.19 s^{-1}	11a 60.32 s^{-1}	12a 108.5 s^{-1}
6mm/12μm	0.1	0(single)	0.110 0.127	0.093	0.796		1.025		1.681
	0.1	20	0.274 0.580	0.265	0.314	0.403 0.429	0.559	0.750 1.252	0.941 1.594
	0.1	24	0.089 0.279	0.276	0.279	0.318	0.477 0.711	0.520 1.360	0.742 1.179
	0.1	30	0.169 0.217	0.251	0.188	0.256 0.548	0.335 0.385	0.404 0.543	0.430 0.445
3mm/12μm	0.1	0(single)	0.599	0.656	0.934 1.018	1.032	1.425		1.824 2.098
	0.1	20	0.433	0.478	0.402	0.516 0.713	0.870	1.040 1.382	1.670 1.720
	0.1	24	0.293	0.281	0.371	0.449	0.665	0.988	1.270 2.341
	0.1	30	0.252	0.237 0.312	0.263 0.332	0.304 0.423	0.477	0.588 0.738	0.629 0.926
6mm/8μm	0.1	0(single)	0 0	0	0	0	0	0.642 0.658	1.565

	0.1	20	0.142 0.187	0.159	0.214	0.273	0.437 0.786	0.538	0.698
	0.1	24	0.115 0.133	0.131 0.290	0.174	0.225	0.336 0.801	0.361	0.484
	0.1	30	0.077	0.152 0.307	0.128	0.168 0.202	0.251 0.393	0.252	0.307 0.717

***F*=0.24%**

Fiber	*F*, %	*P*, %	v_s, mm/s						
			Quiescent $\dot{\gamma}=0$	4a 1.34 s^{-1}	6a 4.02 s^{-1}	8a 12.06 s^{-1}	10a 36.19 s^{-1}	11a 60.32 s^{-1}	12a 108.5 s^{-1}
6mm/12μm	0.24	0(single)	0.110 0.127	0	0	0	0	0)	0
	0.24	20	0.117	0.103	0.149	0.228 0.294	0.320 0.356	0.412 0.462	0.611 0.484
	0.24	24	0.099	0.113	0.105	0.274	0.299	0.369 0.439	0.426
	0.24	30	0.111	0.099	0.123	0.169	0.204 0.335	0.203 0.328	0.263 0.365
3mm/12μm	0.24	0(single)	0.308 0.342	0.430 0.431	0.525	0.535	0.432 1.553		2.097
	0.24	20	0.206	0.204 0.289	0.205 0.359	0.306	0.360 1.06	0.467	0.803
	0.24	24	0.134 0.150	0.156	0.193 0.261	0.250 0.268	0.320 0.990	0.447 0.533	0.508
	0.24	30	0.096	0.138	0.148 0.175	0.224	0.227 0.475	0.318 0.394	0.416
6mm/8μm	0.24	0(single)	0	0	0	0	0	0	
	0.24	20	0.032	0.044	0.039	0.116	0.172	0.169 0.231	0.217
	0.24	24	0.023	0.021	0.042	0.048 0.076	0.104	0.123 0.316	0.183
	0.24	30	0.024	0.034	0.037	0.058	0.082	0.145	0.100

***F*=0.4%**

Fiber	*F*, %	*P*, %	v_s, mm/s						
			Quiescent $\dot{\gamma}=0$	4a 1.34 s^{-1}	6a 4.02 s^{-1}	8a 12.06 s^{-1}	10a 36.19 s^{-1}	11a 60.32 s^{-1}	12a 108.5 s^{-1}
6mm/12μm	0.4	0(single)	0	0	0	0.052	0	0.197	
	0.4	20	0.054 0.057	0.091 0.115	0.095 0.216	0.098 0.202	0.179 0.181	0.186 0.318	0.252 0.352
	0.4	24	0.053	0.068 0.079	0.121	0.107	0.151	0.184	0.169
	0.4	30	0.026	0.077	0.139	0.121 0.188	0.161	0.161 0.166	0.139 0.189

3mm/12μm	0.4	0(single)	0.024 0.179	0	0.045	0.118		0.866	1.413
	0.4	20	0.119	0.189	0.192	0.204	0.303	0.396 0.521	0.448 0.685
	0.4	24	0.089	0.131 0.157	0.162	0.262	0.311	0.362	0.480 0.617
	0.4	30	0.080	0.142 0.284	0.142 0.159	0.236	0.256	0.315	0.333
6mm/8μm	0.4	0(single)	0	0	0	0	0.450 0.6560	0	0
	0.4	20	0.007 0.013	0.024	0.019	0.035	0.069	0.057	0.076 0.104
	0.4	24	0.011 0.012	0.017	0.020	0.032	0.058	0.059	0.084
	0.4	30	0.023 0.0523	0.028 0.118	0.022	0.055 0.102	0.041 0.043	0.049	0.066 0.207

Several values of the sedimentation velocity for certain tests allowed to estimate absolute error of the measurement as a mean magnitude of the standard deviations in the certain tests. This mean magnitude defines absolute error of the measurement as σ~0.12076 mm/s. However data analysis shows that the absolute level of fluctuations of the velocity measurements depends on the velocity, whereas the relative level of velocity fluctuations remains approximately constant. Therefore it was assumed that measurements error is defined by relative magnitude of the standard deviation which is estimated δv_s~27.06%. Note that this magnitude presents only random error of the single measurement but not includes the error which is related with suspension preparation.

Data of Table 5 are also presented in Fig. 7. Plots present the sedimentation velocities v_s as a function of shear rate $\dot{\gamma}$. Linear fitting is used for averaging the experimental dependencies. All plots demonstrate that maximum deceleration of sedimentation is provided by the long and thin fibers 6mm/8μm. Short and thick fibers 3mm/12μm have a minimum effect on sedimentation.

Obviously the effect of fiber type on sedimentation velocity resembles the effect of fiber type on a shear stress (or viscosity). A maximum effect on shear stress as well as on sedimentation rate is proved by the long and thin fibers 6mm/8μm. Short and thick fibers 3mm/12μm have a minimum effect on shear stress as well as on sedimentation rate. Long and thick fibers 6mm/12μm show intermediate influence.

Observed similarity compares well with the statement that sedimentation rate is inversely proportional to the actual shear viscosity of the suspension (Bazilevsky et al. 2016). The statement is based on the concept of self-consistent field. The statement was validated by experiments with fiber suspensions on the basis of glycerol. Presented below sedimentation graphs correlate well with the rheological graphs in the framework of the statement regarding relation between sedimentation and rheology.

Fig. 10a shows the dependences of sedimentation rate v_s versus fiber mass concentration F (left plots) and versus overlap parameter cl^3 (right plots). The plots were obtained for all studied fibers (6mm/12μm, 3mm/12μm, 6mm/8μm), for shear rates $\dot{\gamma}$=0, 1.34, 4.02, 12.06, 36.19, 60.32, 108.5 s^{-1} and particles volume concentration P=24%. The Fig. 10b shows the same data in 3D format.

One can conclude that on the left graphs ($v_s(F)$) the points for 6mm/12μm, 3mm/12μm, 6mm/8μm demonstrate essentially different sedimentation for fibers of different type. For example, typically points for fibers 6mm/8μm are located below points for fibers 3mm/12μm. The points for fibers 6mm/12μm tend to occupy intermediate positions. On the other hand the points on the right graphs ($v_s(cl^3)$) are accumulated along a single curve by a chaotic manner independently on fiber geometry. Thus the effect of fiber type on the sedimentation becomes qualitatively indistinguishable in the framework of the presentation $v_s(cl^3)$.

The dependencies in Fig. 10a were fitted by hyperbola v_s=Y0/(1+TETA*x), where x=F or x=cl^3. This function is an inverse linear dependence. (The assumption follows from approximately linear dependences in Fig. 9). The transition from the dependency v_s versus F (left graphs) to the dependency v_s versus cl^3 (right graphs) improves remarkably the χ^2-fitting statistics (Chi^2/DoF) in the framework of Origin graphics software package[1] (shown on the plots). The magnitudes χ^2~1 for the dependencies $v_s(cl^3)$ validate the statement of independence of the relation $v_s(F)$ on fiber geometry. Otherwise a large magnitudes χ^2 for the dependencies $v_s(F)$ reject the assumption about independence of the relation $v_s(F)$ on fiber geometry (Taylor 1997).

The dependence of a sedimentation velocity versus an inverse magnitude of shear viscosity was constructed to validate the correlation between the sedimentation process and the viscosity of suspension - Fig. 11. The plot confirms hypothesis about correlation between suspension viscosity and sedimentation velocity. As the first approximation the dependence is linear and described approximately by the Stokes formula (line in Fig. 11)

---

[1] The aim of the fitting procedure is to find those values of the parameters which best describe the data. The standard way of defining the best fit is to choose the parameters so that the sum of the squares of the deviations of the theoretical curve(s) from the experimental points for a range of independent variables:

$$\chi^2(p_1, p_2, \ldots) = \frac{1}{n^{eff} - p} \sum_i \sum_j w_{ji} \left[y_{ji} - f_j(x_{1i}, x_{2i}, \ldots; p_1, p_2, \ldots) \right]^2$$

is at its minimum. Here, y_{ji} are the measured values of the dependent (output) variable y_j for the values of the independent (input) variables $x_1 = x_{1i}$, $x_2 = x_{2i}$, ...; n^{eff} is the total number of experimental points used in the fitting, and p is the total number of adjustable parameters used in the fitting (the difference $d = n^{eff} - p$ is usually referred to as the number of degrees of freedom).

The quantities w_{ji} represent the weights of each experimental point. Four different weighting methods are supported by Origin:

No weight: $w_{ji} = 1$.

Instrumental weights: $w_{ji} = 1/\sigma_{ji}^2$, where σ_{ji} are the error bar sizes stored in error bar columns.

Statistical: $w_{ji} = 1/y_{ji}$.

$$v_s = d_p^2 g(\rho_p - \rho_g)/(18\mu), \qquad (2.2)$$

where μ is the actual viscosity of the suspension.

Additionally, the experimental points were fitted by linear (relatively μ^{-1})) function

$$v_s = A/\mu, \qquad (2.3)$$

where A is the fitting parameter. The fitting statistics including correlation coefficient R^2 is presented in Fig. 11. There is some difference between curves (2.2) and (2.3), which can be caused by random error in sedimentation measurements as well as influence by other factors outside the concept of self-consistent field. Therefore further theoretical explanation of observed

---

[2] If we have a series of n measurements of X and Y written as x_i and y_i where $i = 1, 2, ..., n$, then the *sample correlation coefficient* can be used to estimate the population Pearson correlation r between X and Y. The sample correlation coefficient is written

$$r_{xy} = \frac{\sum_{i=1}^{n}(x_i - \bar{x})(y_i - \bar{y})}{(n-1)s_x s_y} = \frac{\sum_{i=1}^{n}(x_i - \bar{x})(y_i - \bar{y})}{\sqrt{\sum_{i=1}^{n}(x_i - \bar{x})^2 \sum_{i=1}^{n}(y_i - \bar{y})^2}},$$

where x and y are the sample means of X and Y, and s_x and s_y are the sample standard deviations of X and Y.

This can also be written as:

$$r_{xy} = \frac{\sum x_i y_i - n\bar{x}\bar{y}}{(n-1)s_x s_y} = \frac{n\sum x_i y_i - \sum x_i \sum y_i}{\sqrt{n\sum x_i^2 - (\sum x_i)^2}\ \sqrt{n\sum y_i^2 - (\sum y_i)^2}}.$$

If x and y are results of measurements that contain measurement error, the realistic limits on the correlation coefficient are not −1 to +1 but a smaller range

The Pearson correlation is +1 in the case of a perfect positive (increasing) linear relationship (correlation), −1 in the case of a perfect decreasing (negative) linear relationship (**anticorrelation**), and some value between −1 and 1 in all other cases, indicating the degree of linear dependence between the variables. As it approaches zero there is less of a relationship (closer to uncorrelated). The closer the coefficient is to either −1 or 1, the stronger the correlation between the variables.

effects requires consideration of the micromechanical processes of the fiber-fiber and fiber-particle interaction in the shear flow. In particular, the collective effects of the friction between fibers and particles, elastic deformation of the fibers, hydrodynamical and contact interaction between fibers and particles should be considered experimentally and theoretically to obtain the constitutive equation of particle sedimentation in fiber-containing liquids.

Conclusions

1. Particle sedimentation in guar gum with fibers PLA2mod of different geometry is characterized by a number of remarkable features in the case when liquid is subjected to shear flow. In particular, the particle sedimentation velocity in guar gum laden with fibers under consideration, increases with an increase in the shear rate and decreases with an increase in particle and fiber concentration. Unlike the case of glycerol, the addition of fibers into guar gum results in significant decrease of the particle sedimentation velocity over the whole range of shear rates ~1÷100 s^{-1}. As the first approximation, the sedimentation velocity is described by the Stokes formula, where the viscosity is equal to the actual suspension viscosity at a certain sear rate.

2. At a fixed mass concentration *F,* long and thin fibers 6mm/8μm provide the maximum increase in the viscosity and the maximum decrease in the sedimentation velocity as compared to the long and thick fibers 6mm/12μm and short and thick fibers 3mm/12μm. The latter type of fibers (3mm/12μm) provides minimum increase in the viscosity and minimum decrease in the sedimentation velocity as compared to other types of the fibers.

3. At a fixed value of overlap parameter cl^3, all studied fibers

provide the same increase in the viscosity and the same decrease in the sedimentation velocity independently on a fiber gemetry and mass concentration.

Acknowledgments The work was conducted under Research Contract No. Slb-FAC-24/01/2014-IPM_RAN/TCS between Schlumberger Technology Corporation and the A. Ishlinsky Institute for Problems in Mechanics, RAS. The authors thank Professor R.V. Goldstein for the help in the work.

REFERENCES

Barnes H.A., Hutton J.F., Walters K. An introduction to rheology. Amsterdam, Elsevier, 1989.

Bazilevsky A.V., Kalinichenko V.A., Plyashkevich V.A., Badazhkov D.V., Rozhkov A.N. Sedimentation of particles in shear flows of fluids with fibers // Rheologica Acta. 2016. V. 55. № 1. P. 11-22.

Bazilevskii A.V., Rozhkov A.N. Motion of a sphere down an inclined plane in a viscous flow // Fluid Dynamics. 2009. V. 44. № 4. P. 566-576.

Bazilevskii A.V., Koroteev D.A., Rozhkov A N., Skobeleva A.A. Sedimentation of particles in shear flows of viscoelastic fluids // Fluid Dynamics. 2010. V. 45. № 4. P. 626-637.

Dogon D., Golombok M. Self-regulating solutions for proppant transport // Journal of Petroleum Science and Engineering. 2016. V. 146. P. 308–317.

Dogon D., Golombok M. Self-regulating solutions for proppant transport // Chemical Engineering Science. 2016. V. 148. P. 219–228.

Elgaddafi R., Ahmed R., George M., Growcock F. Sedimentation behavior of spherical particles in fiber-containing drilling fluids // Journal of Petroleum Science and Engineering. 2012. V. 84-85. P. 20–28.

Gheissary G., van der Brule B.H.A.A. Unexpected phenomena observed in particle sedimentation in non-newtonian media // J. Non-Newtonian Fluid Mech. 1996. V. 67. № 1. P. 1–18.

Harlen O.G., Sundararajakumar R.R., Koch D.L. Numerical simulations of a sphere sedimentation through a suspension of neutrally buoyant fibers // J. Fluid Mech. 1999. V. 388. P. 355–388.

Hinch E.J. Mechanical model of dilute polymer solutions in strong flows // Physics of Fluids. 1977. V. 20. № 10. Pt. 2. P. S22-S30.

Liu Y., Sharma M.M. Effect of fracture width and fluid rheology on particles sedimentation and retardation: an experimental study // SPE/DOE. 2005. № 96208. P. 1–12.

Petrie C.J.S. The rheology of fibre suspensions // J. Non-Newtonian Fluid Mech. 1999. V. 87. № 2–3. P. 369-402.

Roodhart L.P. Particles sedimentation in non-newtonian fracturing fluids // SPE/DOE 1985. № 13905. P. 1–10.

Shalagina A.E., Fu D. Treatment fluid. Patent WO 2015160275 A1. 2015.

Shalagina A.A., Kraemer C., Inozemtseva E.A. Fluide de traitement. Patent WO 2015160277 A1. 2015.

Taylor J.R. An introduction to error analysis the study of uncertainties in physical measurements. University Science, Sausalito, 1997.

van der Brule B.H.A.A., Gheissary G. Effects of fluid elasticity on the static and dynamic sedimentation of a spherical particle // J Non-Newtonian Fluid Mech. 1993. V. 49. № 1. P. 123–132.

Ventura C., Blanco A., Negro C., Ferreira P., Garcia F., Rasteiro M. Modeling pulp fiber suspension rheology // TAPPI Journal. 2007. V. 6. № 7. P. 17-23.

FIGURES

(a)

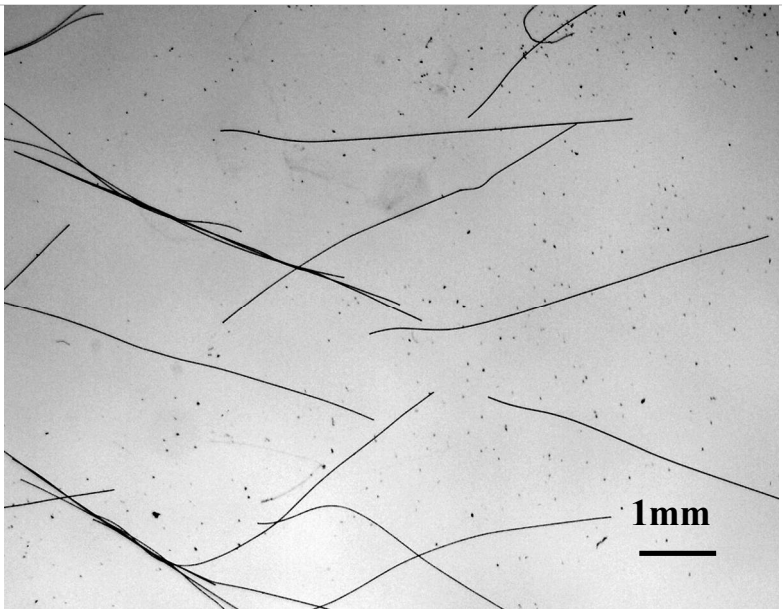

(b)

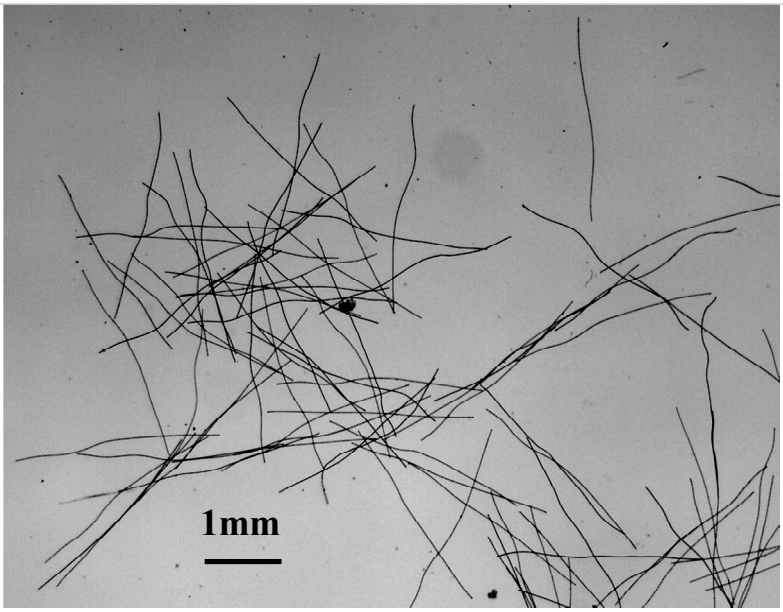

Fig. 1 (beginning)

(c)

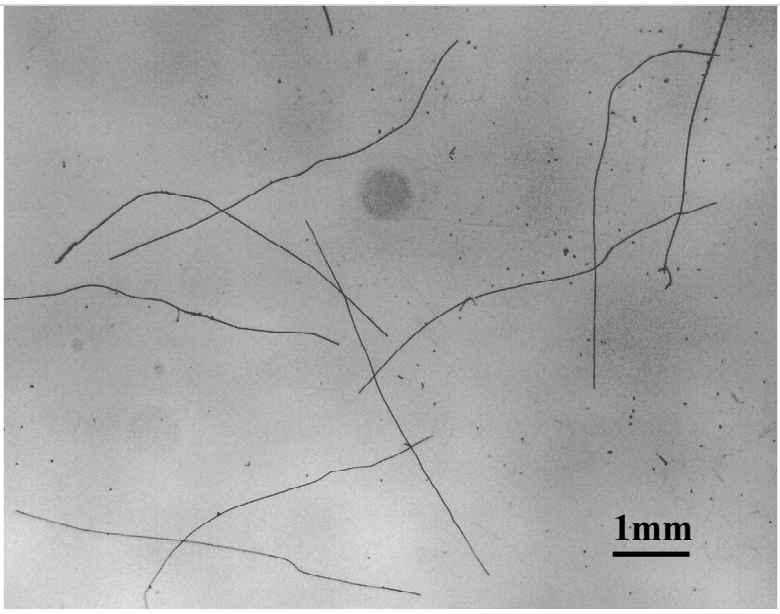

Fig. 1 (end) Microphotographs of dry PLA fibers of different lengths and diameters: **a** - 6mm/12 μm, **b** - 3mm/12μm and **c** - 6mm/8μm

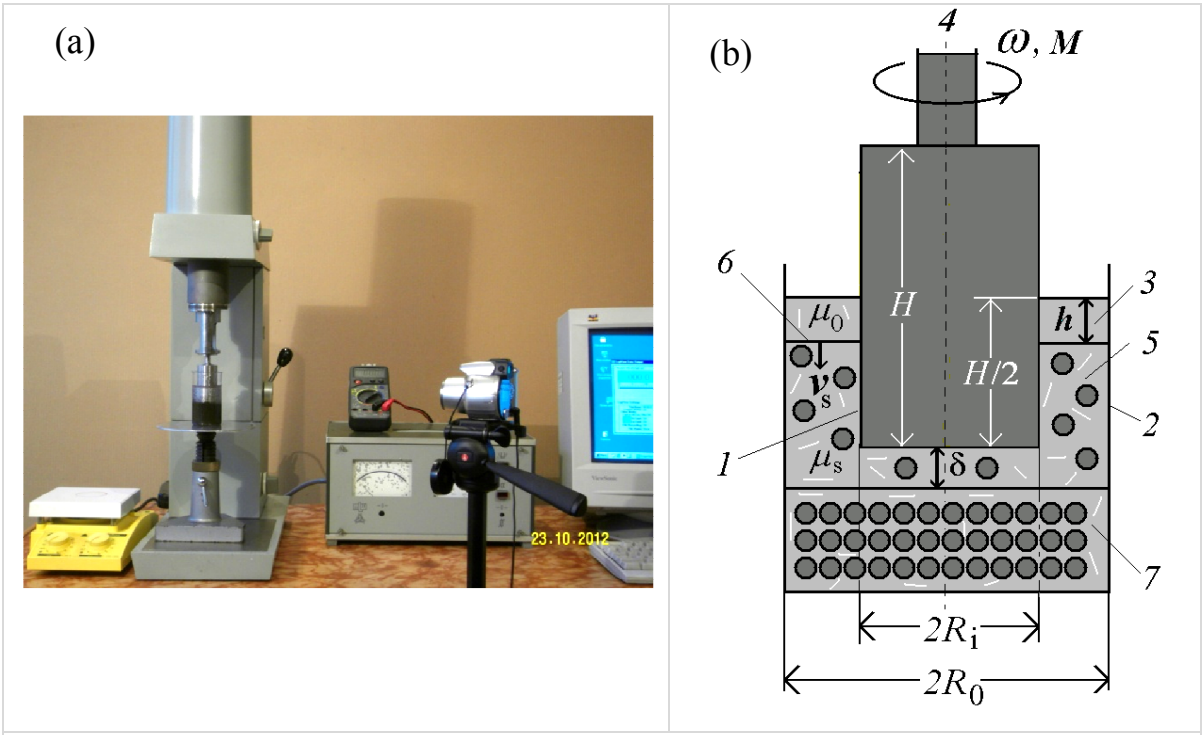

Fig. 2 a Setup LittleBob for investigation of the shear rheology of settling suspensions. **b** Scheme of shear viscosity measurements of fiber-particle suspensions in guar gum (GG): *1* – inner (driven) cylinder, *2* – outer cylinder (a transparent tube), *3* – GG solution without particle, *4* – the drive for rotating the inner cylinder and measuring the applied torque, *5* – the suspension of particle particles and fibers, *6* - sedimentation front, 7 – particle particles at the bottom of the outer cylinder

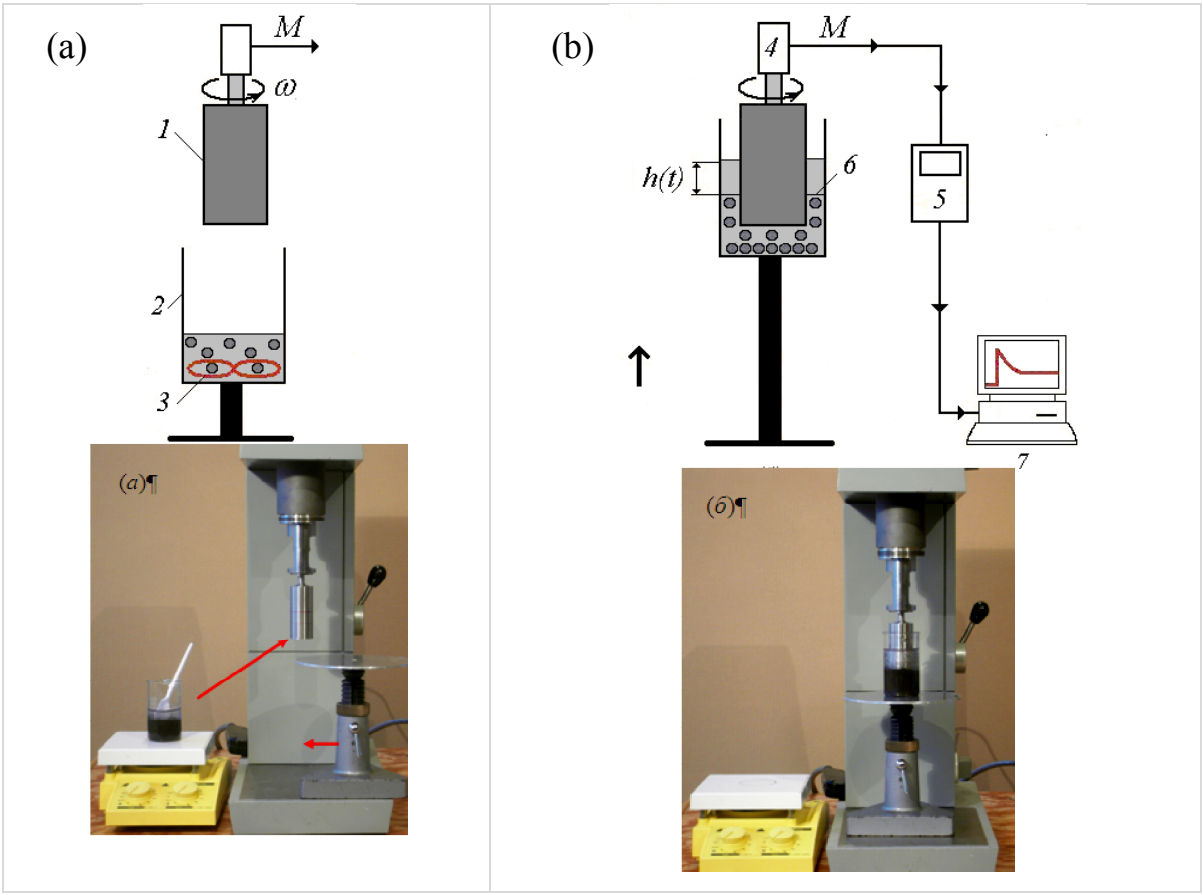

Fig. 3 Scheme of the experimental procedure. **a** Preparation of particle-fiber suspension in the transparent beaker *2* by means of the magnetic stirrer *3* and/or manually. **b** Elevation of the beaker to immerse the inner rotating cylinder *1* into the fluid and fixing the immersion depth by means of the special table with a preset height. Shown: *4* – torque transducer, *5* – digital multimeter, *6* – sedimentation front, *7* – computer

(a)

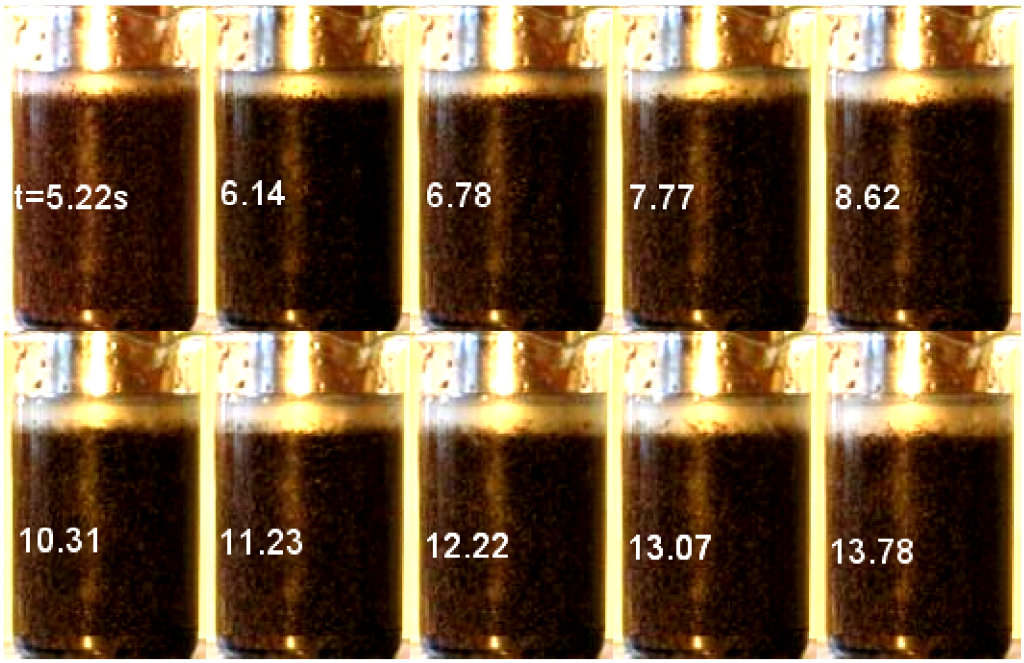

(b)

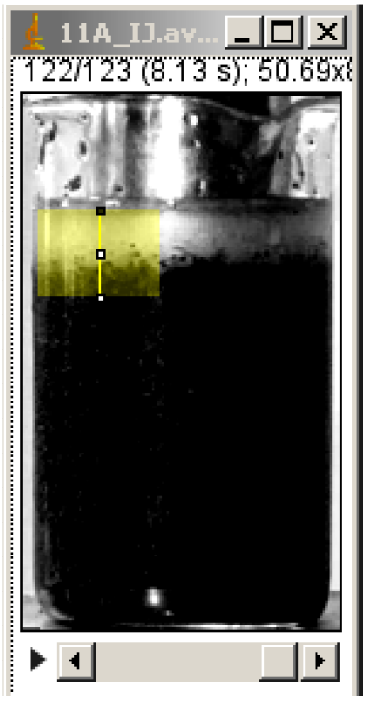

(c)

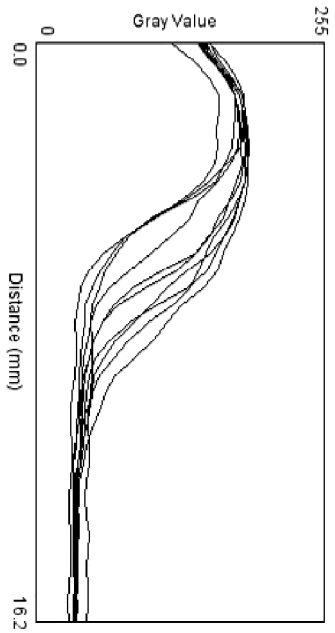

Fig. 4 a The shear- gravitational sedimentation of particles of initial volume concentration P=24% in guar gum GG-0.48% with tested fibers (3mm/12μm) of concentration F=0.24%, 11a, $\dot{\gamma}$=60.32 s^{-1}. **b** The location and width (100 pixels/20 mm) of the measuring line. **c** The set of ten vertical profiles of intensity $I(y)$ defining the position of the front of sedimentation (t=5.22, 6.14, 6.78, 7.77, 8.62, 10.31, 11.23, 12.22, 13.07, 13.78 s)

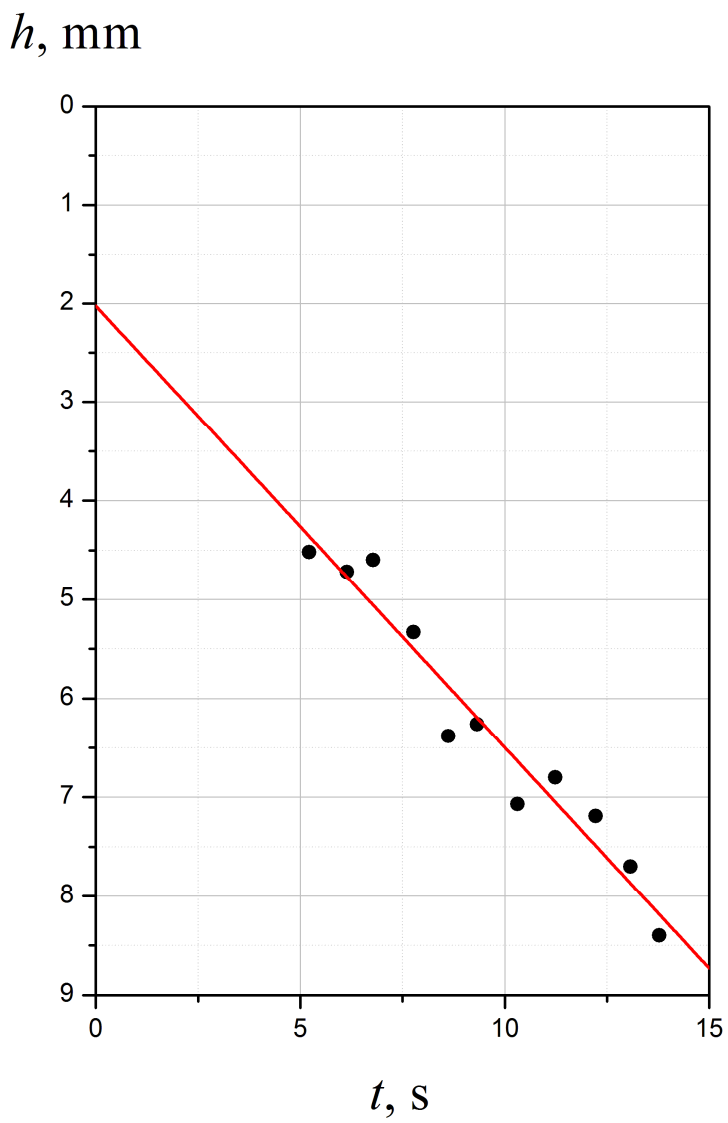

Fig. 5 The front position $h(t)$ of shear-gravitational sedimentation of particles of initial volume concentration P=24% in guar gum GG-0.48% with additives of test fibers 3mm/12μm in shear flow 11a, $\dot{\gamma}$=60.32 s^{-1}. Plot shows the vertical displacement of the sedimentation front with constant velocity v_s=0.447 mm/s

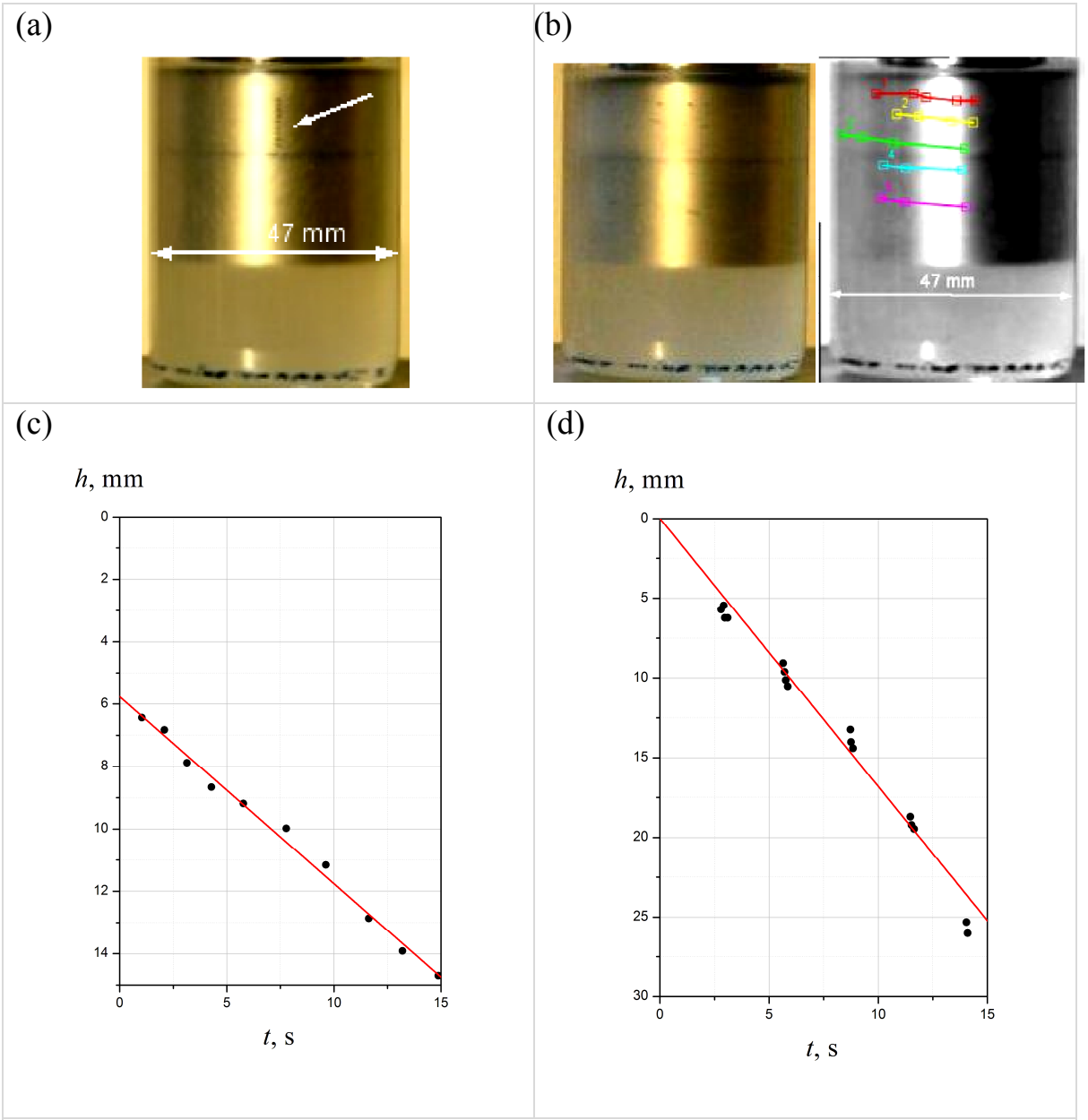

Fig. 6 The deposition of a single particle in guar gum GG-0.48% with test fiber additives F=0.1%: (**a**, **c**) 3mm/12μm, regime quiescent $\dot{\gamma}$=0 s^{-1} and (**b, d**) 6mm/12μm, regime 12a $\dot{\gamma}$=108.6 s^{-1}. Figures **a, b** have been obtained by overlaying the corresponding video frames taken for times: (**a**) t = 1.04, 2.09, 3.14, 4.28,5.77, 7.78, 9.62, 11.63, 13.20,14.87 s and (**b**) t = 3.44, 3.56, 3.62, 3.74, 3.80, 6.29, 6.35, 6.41, 6.50, 9.37, 9,40, 9.49, 9.61, 12.11, 12.17, 12.29, 14.68, 14.74, 14.89 s. Arrow in Fig. 6a shows the particle positions in different moments of time. Figure 6b shows the particles trajectories. The corresponding values of the sedimentation velocity were determined by linear fitting in Figs. 6c and 6d as v_s=0.599 and 1.681 mm/s

F=0 P=0/single, 20, 24, 30%

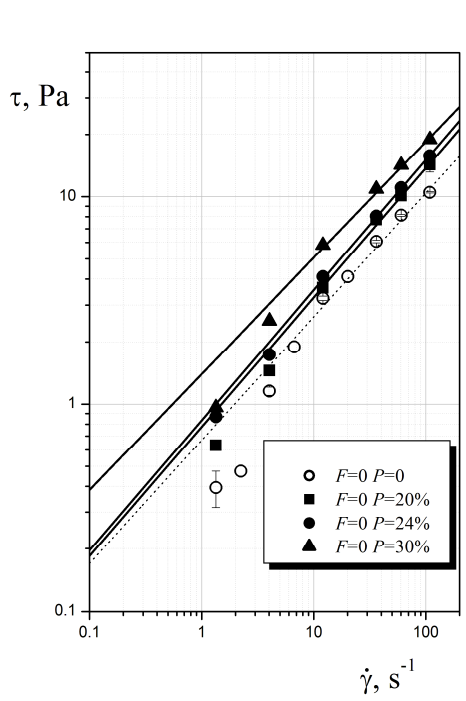

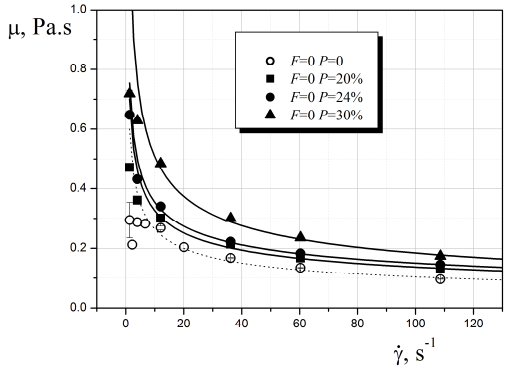

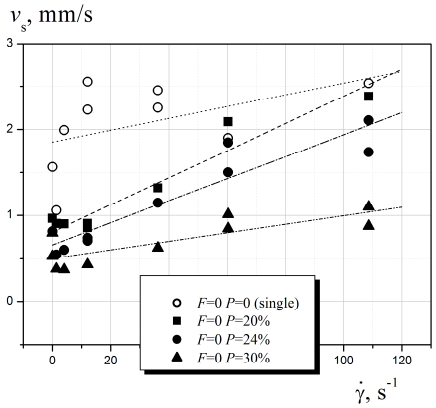

Fig. 7 (beginning)

***F*=0.1% *P*=0/single**

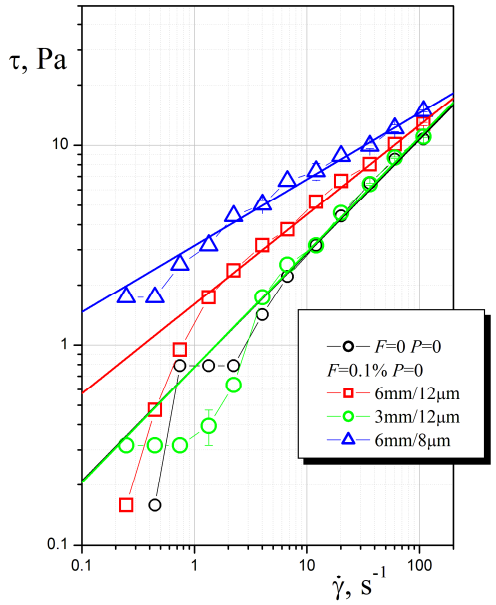

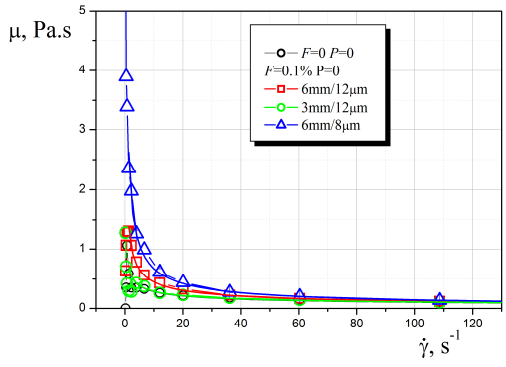

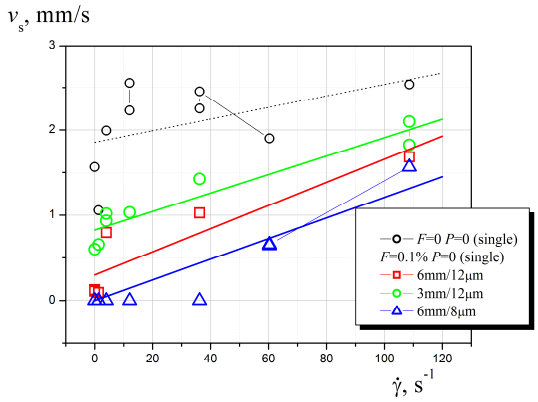

Fig. 7 (continuation)

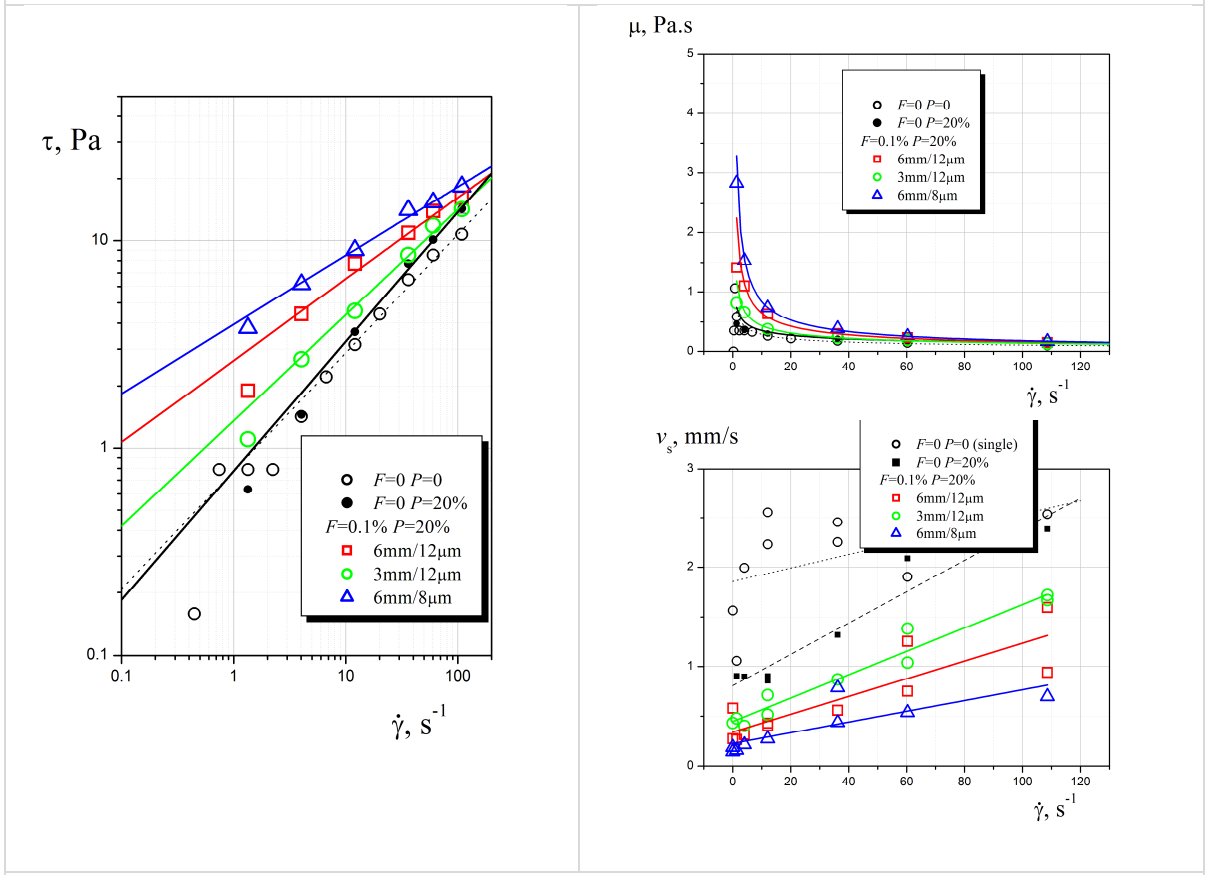

Fig. 7 (continuation)

***F*=0.1% *P*=24%**

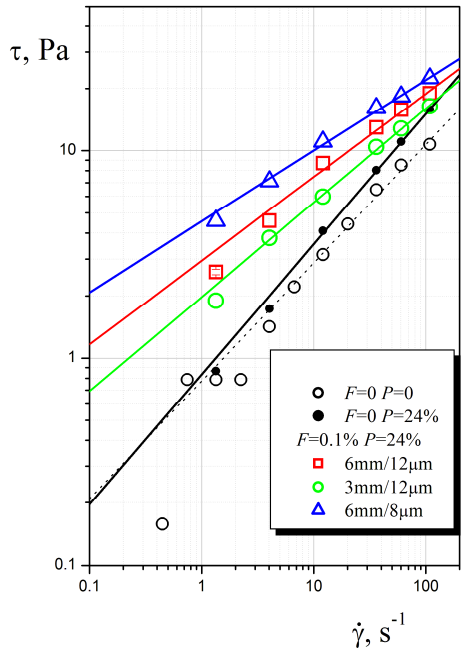

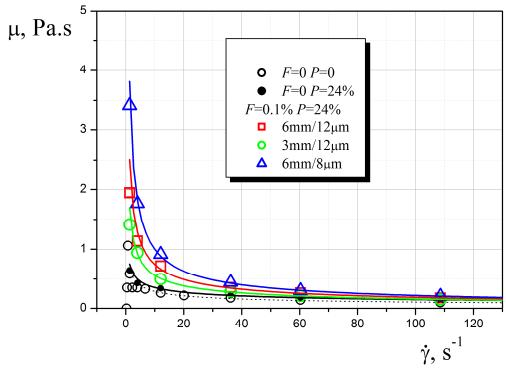

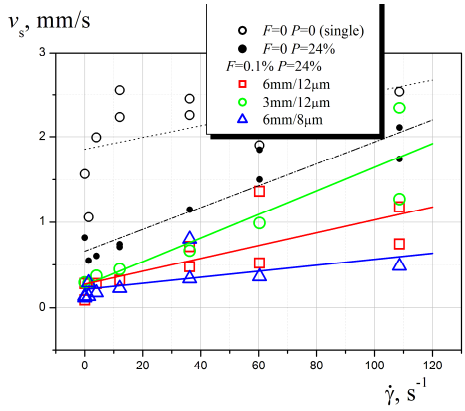

Fig. 7 (continuation)

***F*=0.1% *P*=30%**

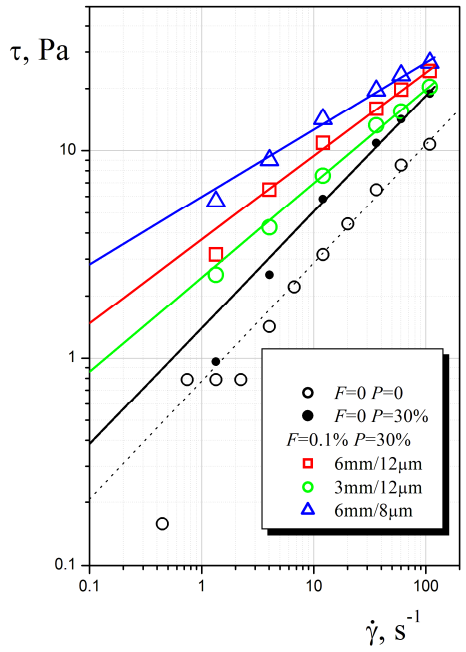

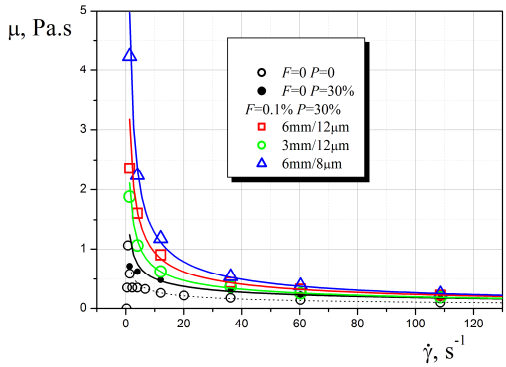

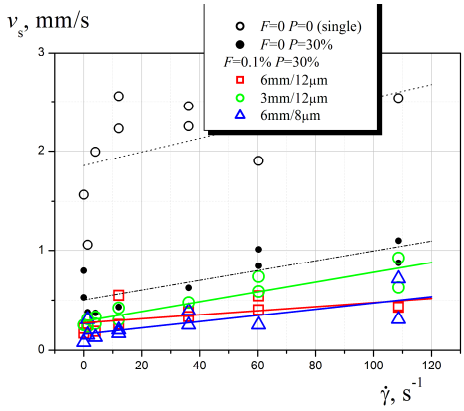

Fig. 7 (continuation)

F=0.24% P=0/single

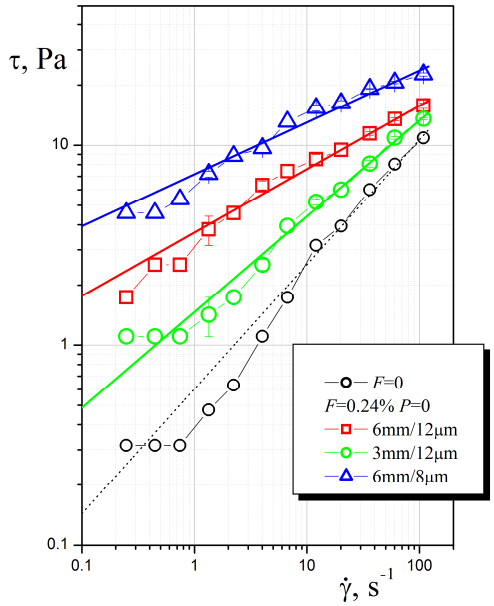

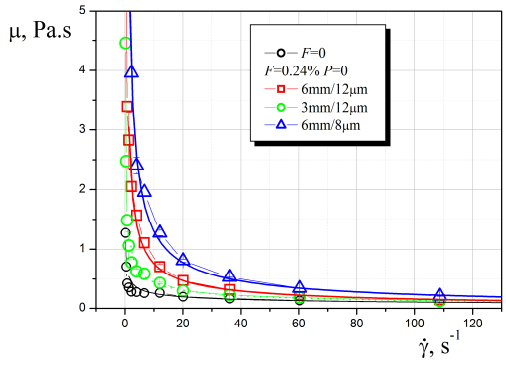

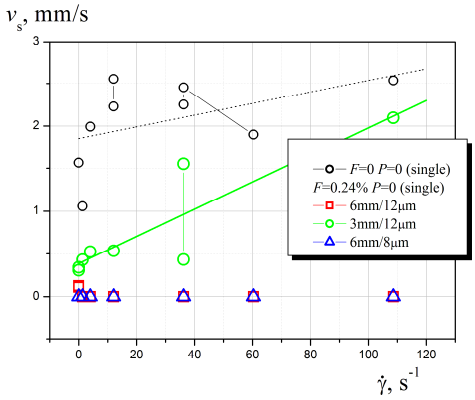

Fig. 7 (continuation)

***F*=0.24% *P*=20%**

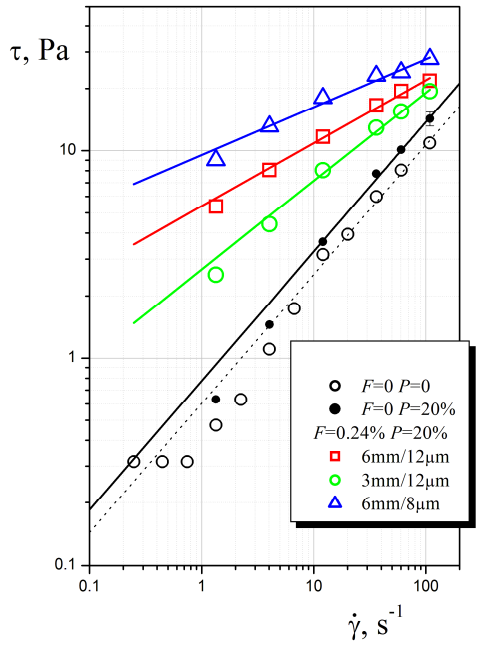

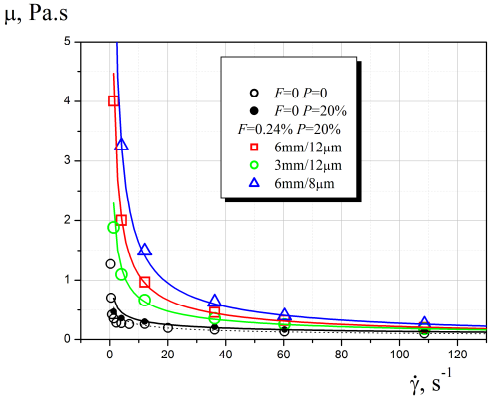

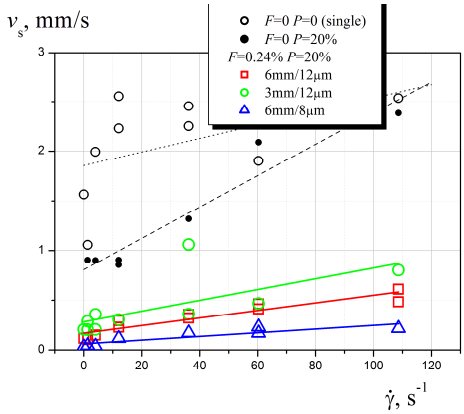

Fig. 7 (continuation)

***F*=0.24% *P*=24%**

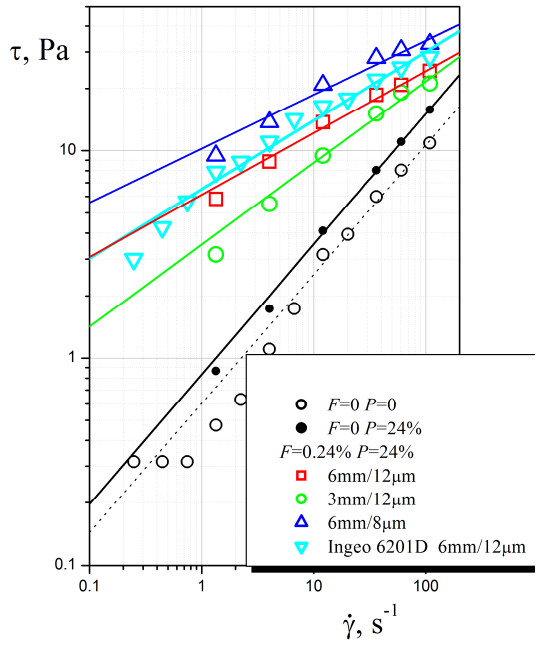

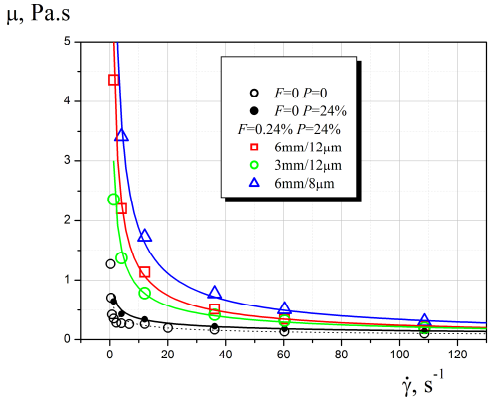

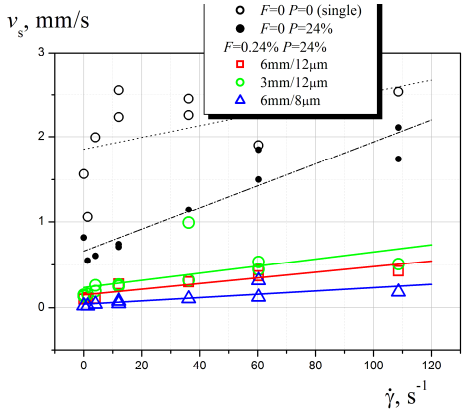

Fig. 7 (continuation)

***F*=0.24% *P*=30%**

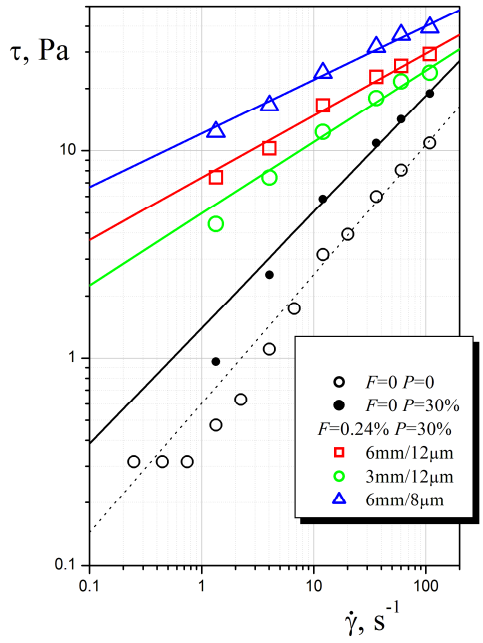

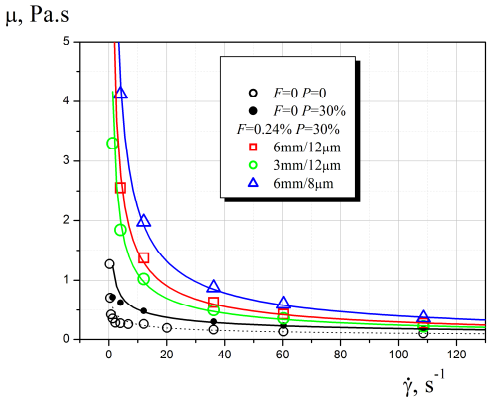

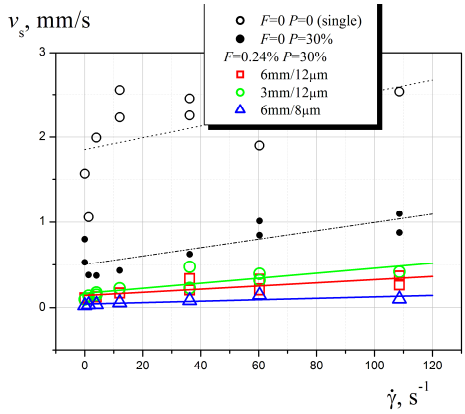

Fig. 7 (continuation)

***F*=0.4% *P*=0/single**

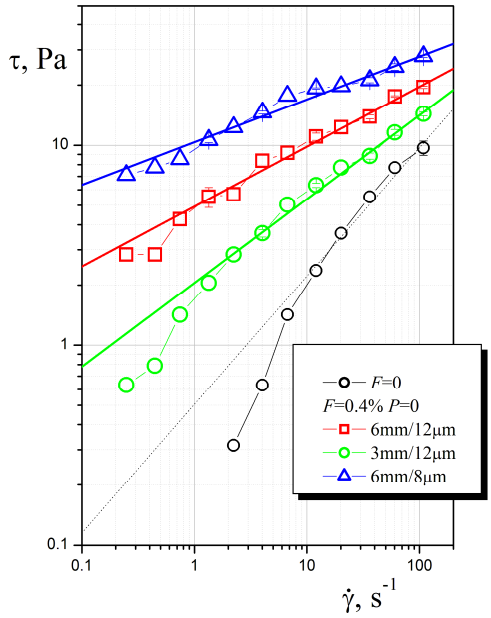

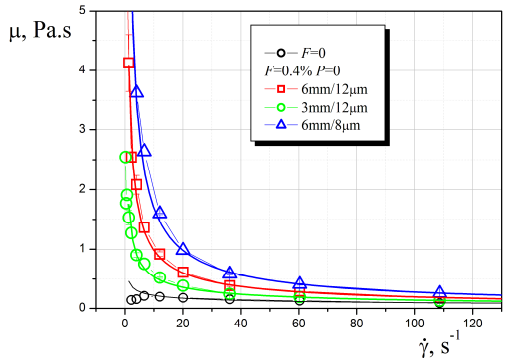

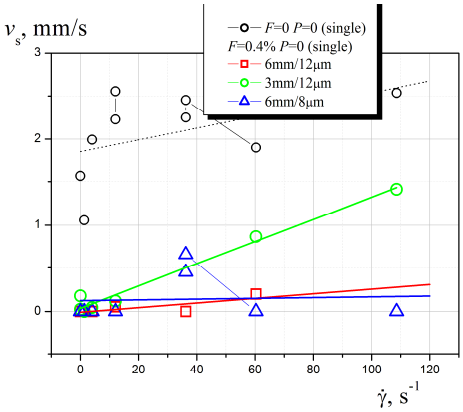

Fig. 7 (continuation)

***F*=0.4% *P*=20%**

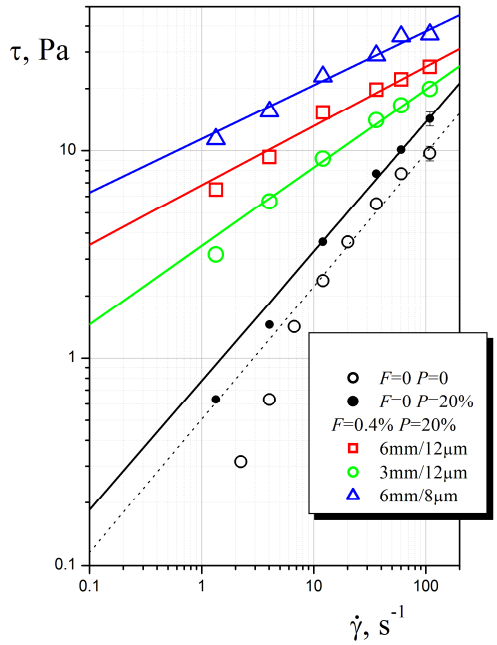

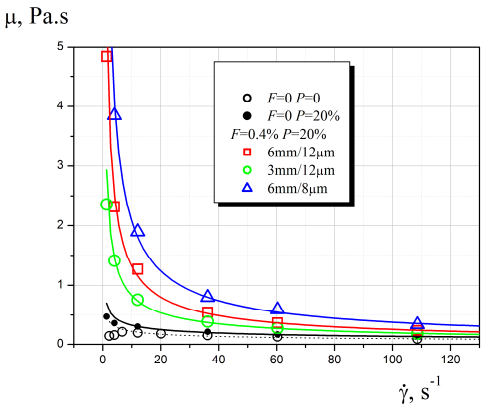

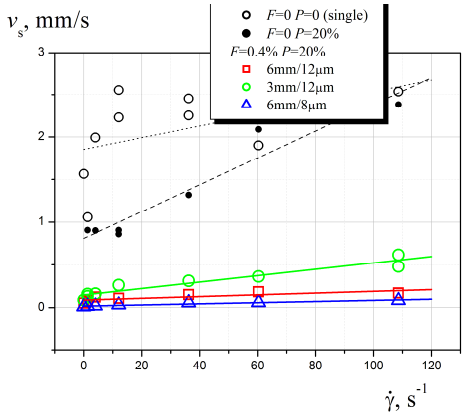

Fig. 7 (continuation)

***F*=0.4% *P*=24%**

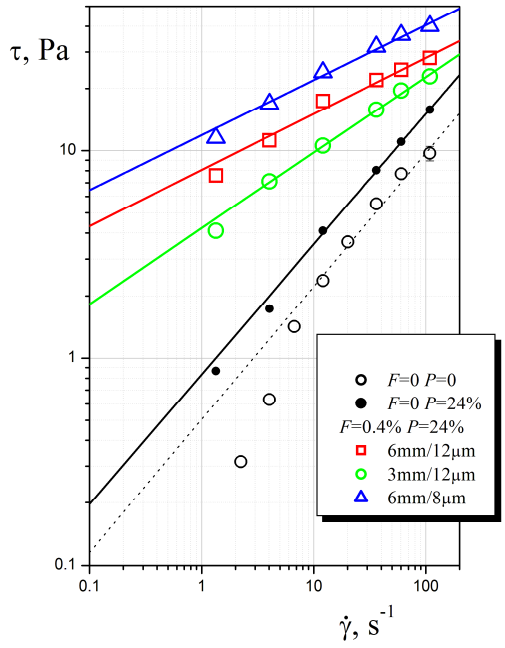

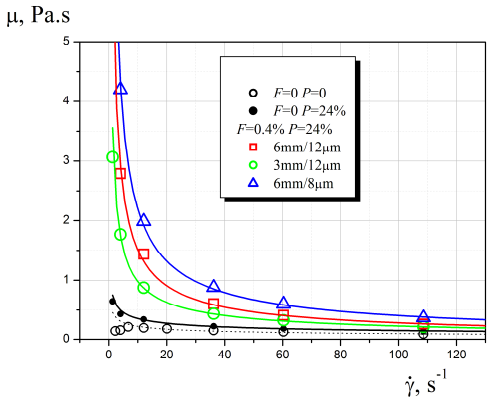

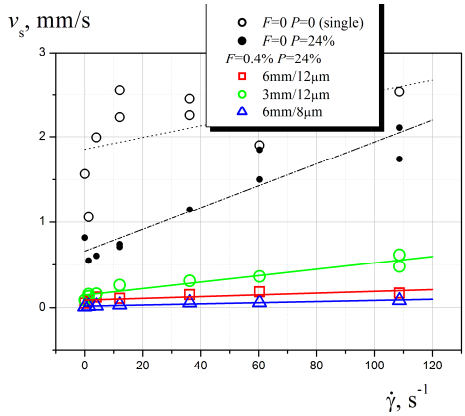

Fig. 7 (continuation)

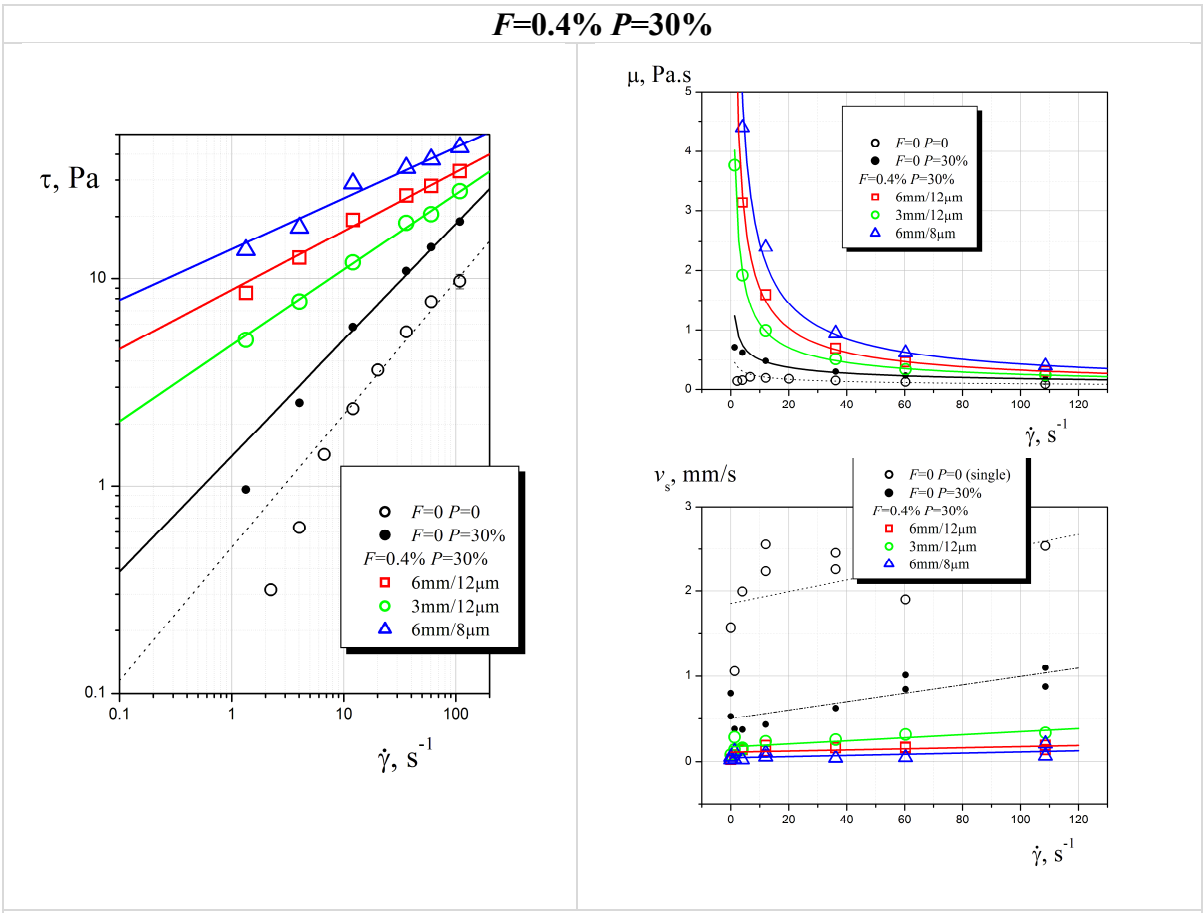

Fig. 7 (end) Effects of fiber geometry on rheology and sedimentation. Shear stress τ, viscosity μ and sedimentation velocity v_s as functions of shear rate $\dot{\gamma}$

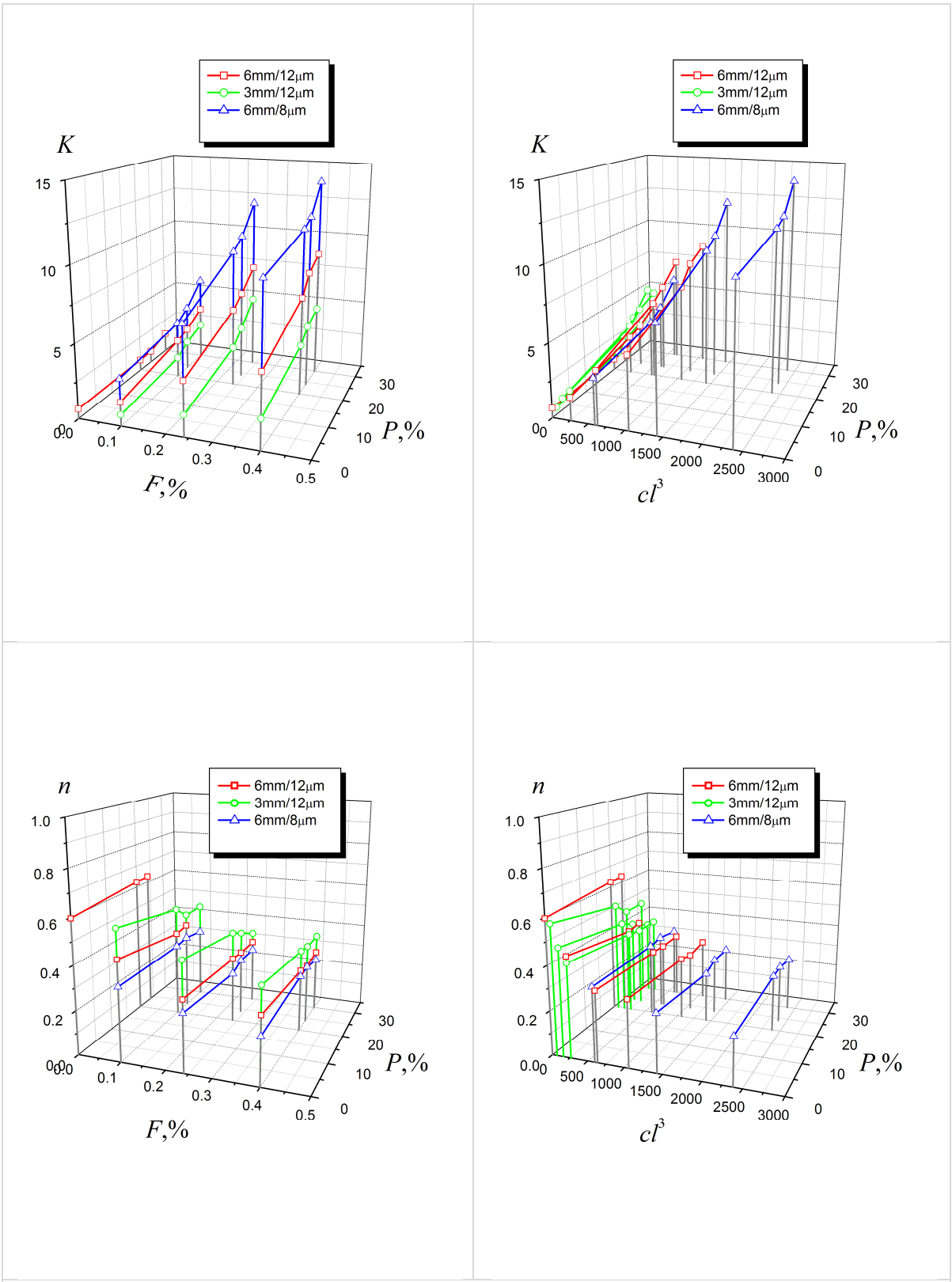

Fig. 8 Left plots represent the consistency K and the flow index n as functions of particle volume concentration P and fiber mass concentration F. Right plots - the same dependences but instead of fiber mass concentration F the average volume fraction cl^3 is used (c is the number of fibers per unit volume and l is the fiber length)

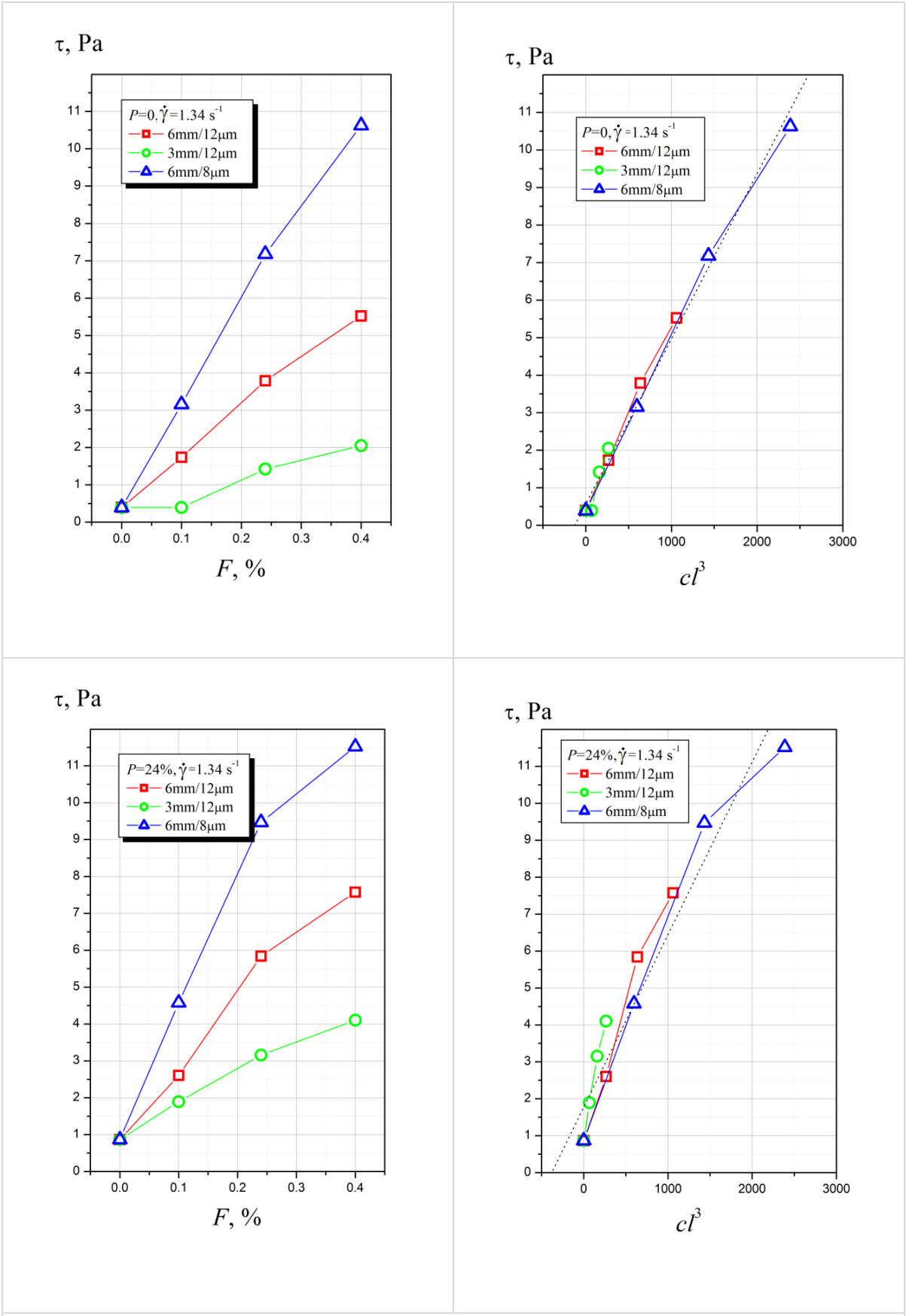

Fig. 9 (beginning)

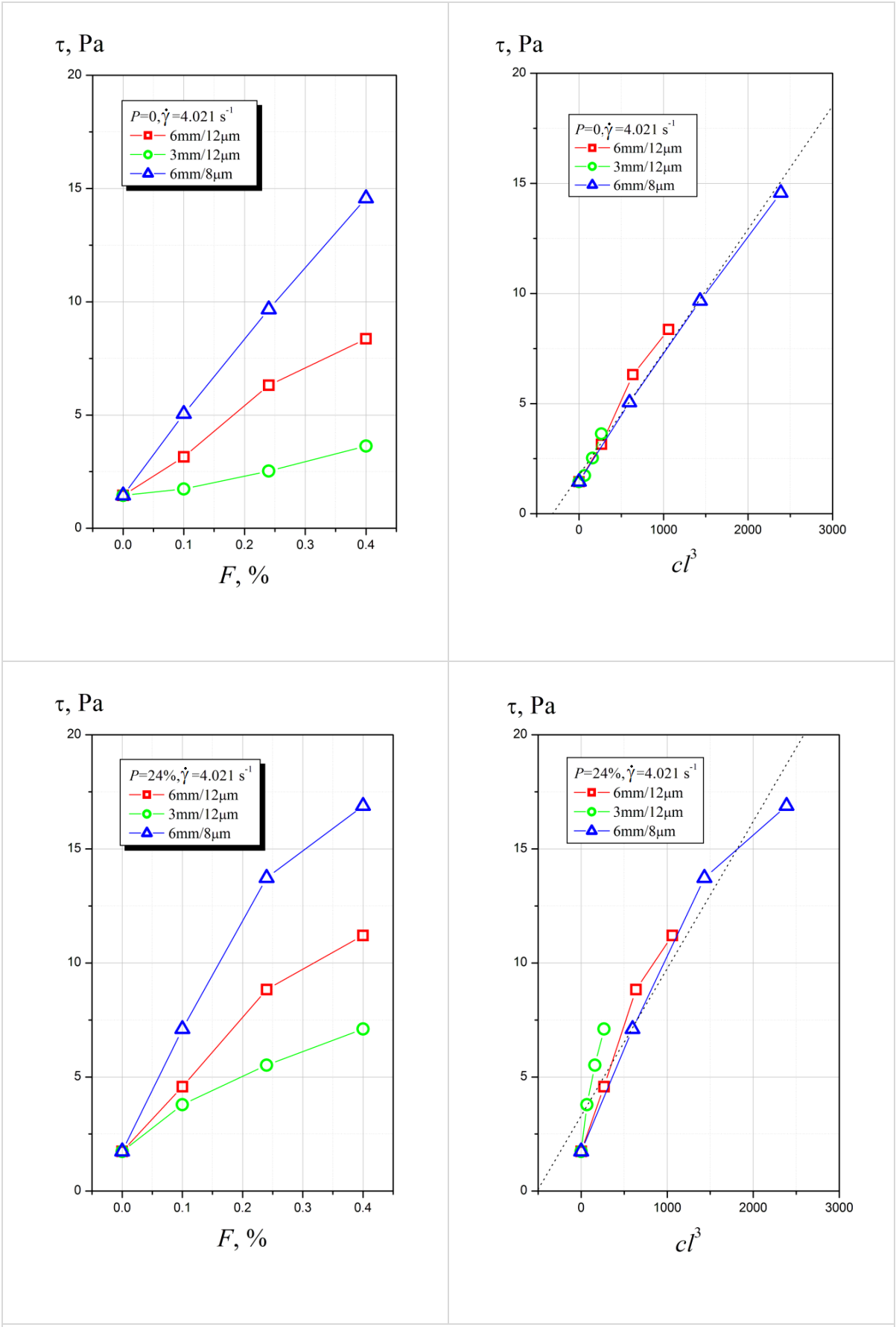

Fig. 9 (continuation)

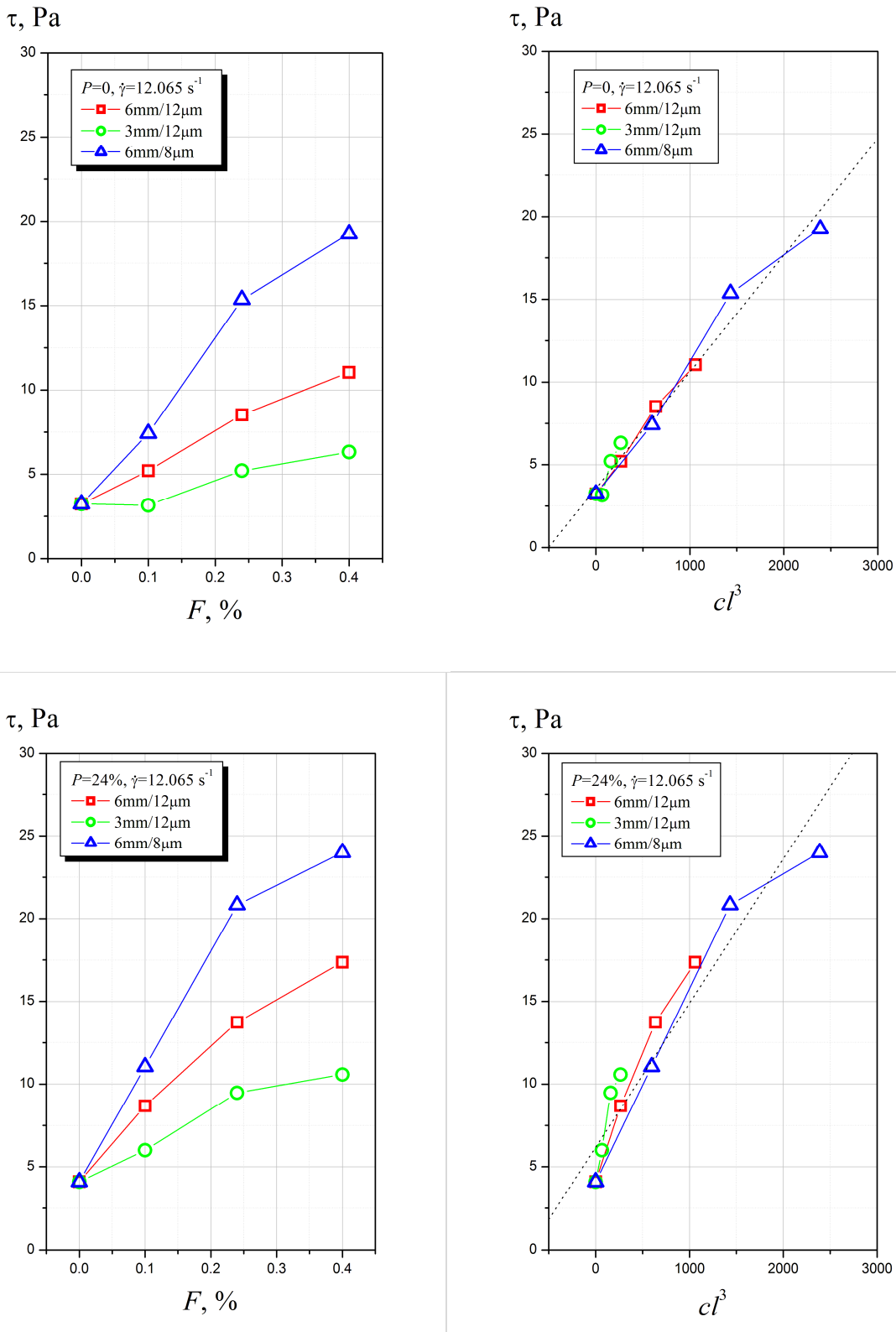

Fig. 9 (continuation)

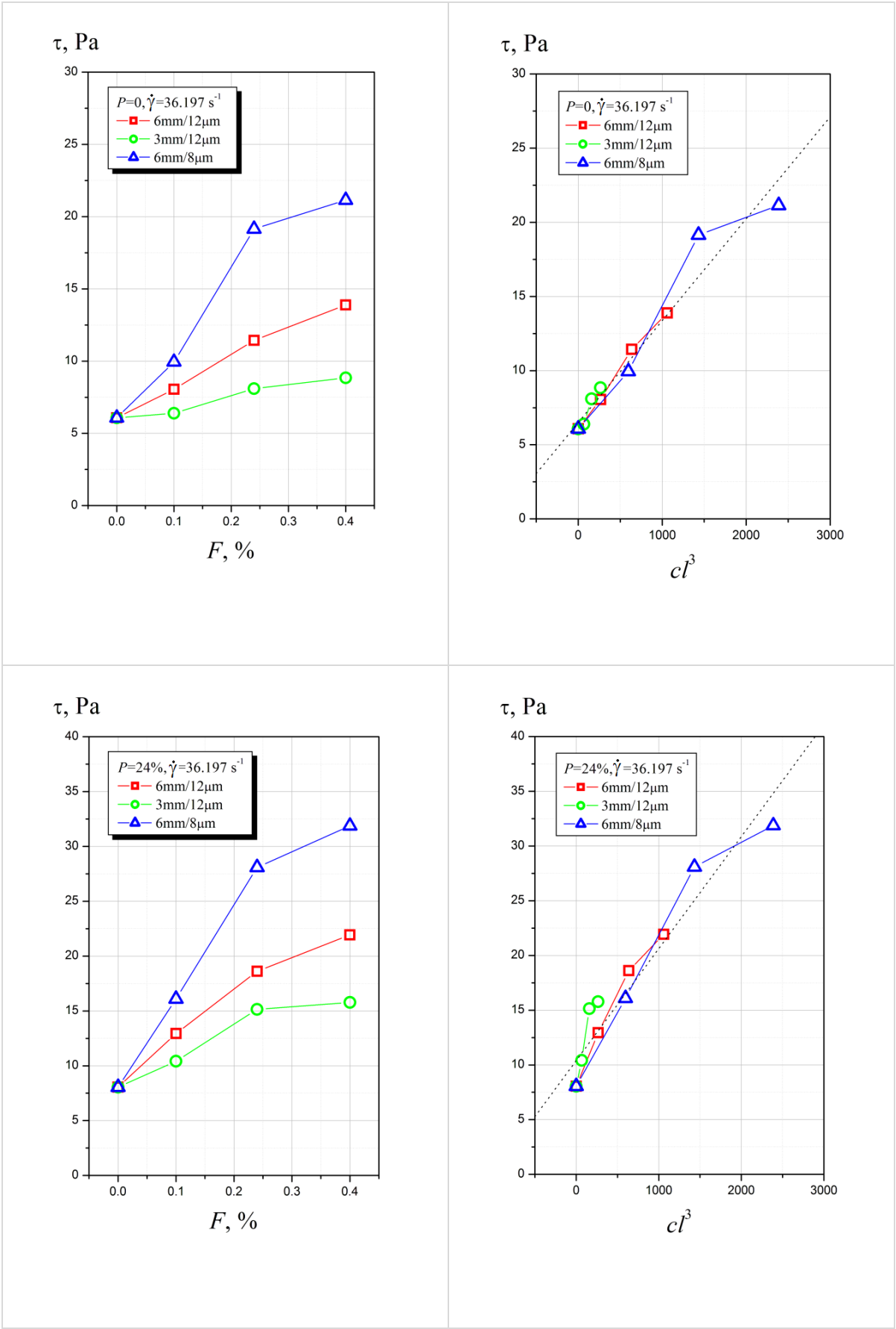

Fig. 9 (continuation)

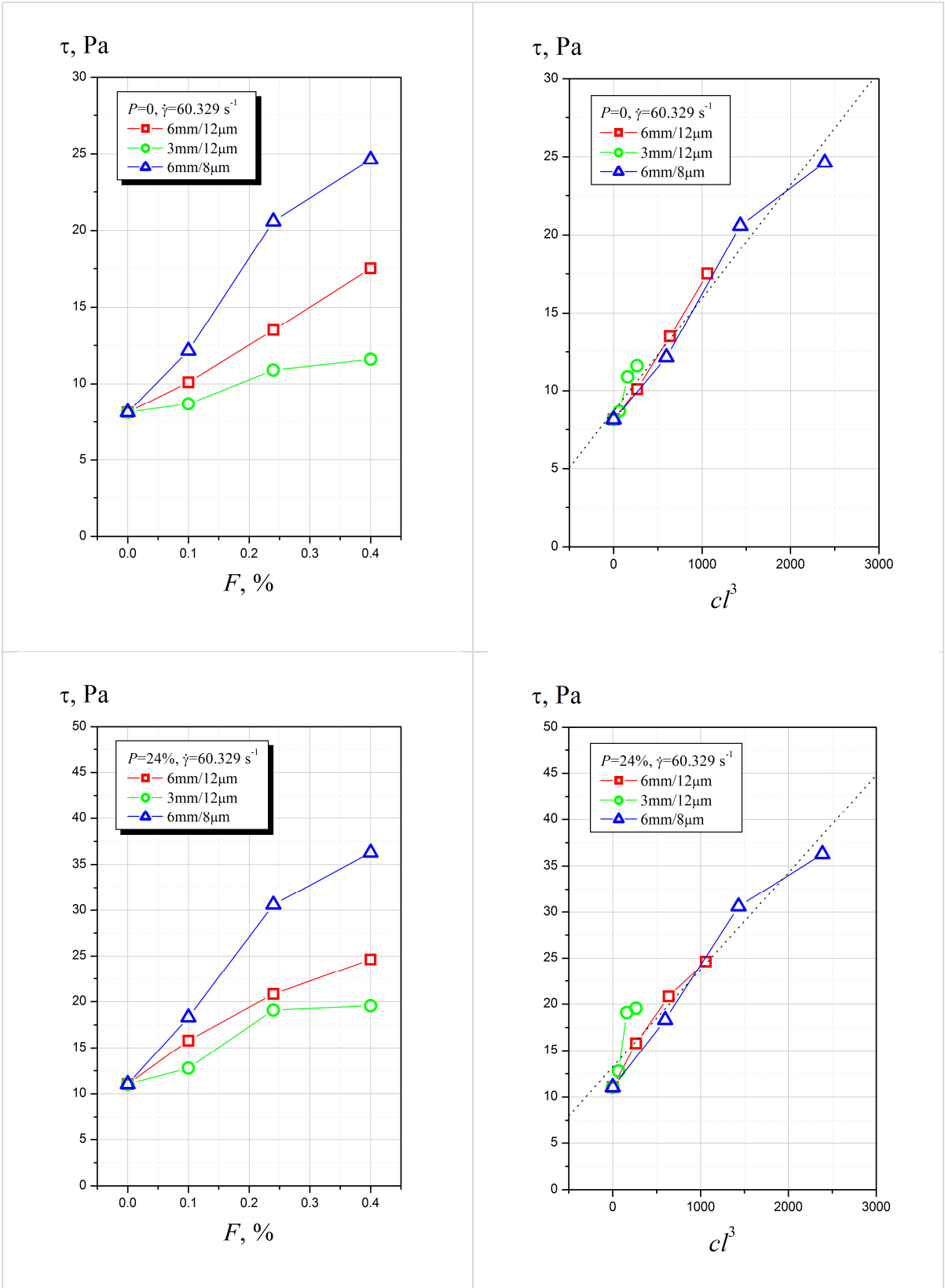

Fig. 9 (continuation)

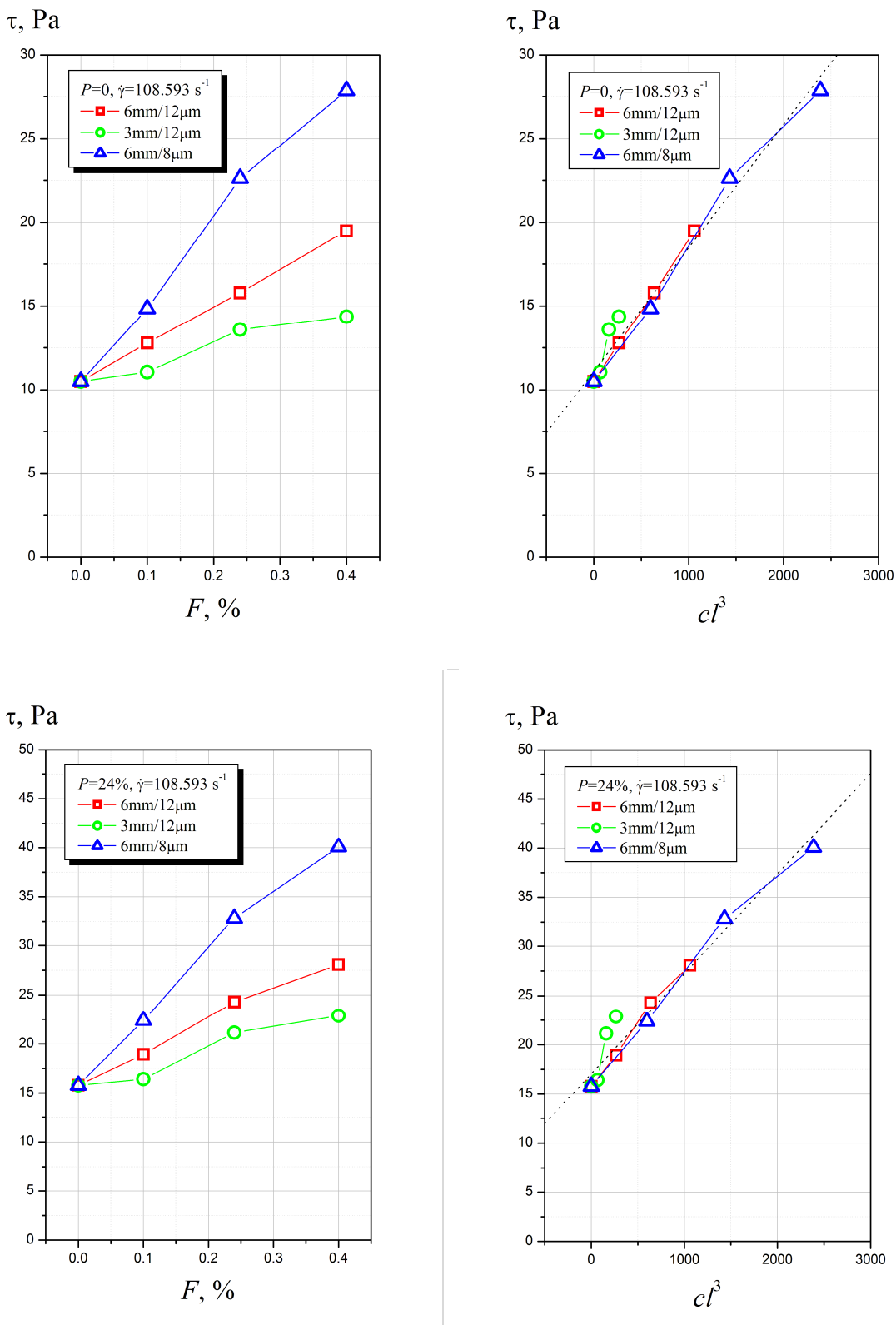

Fig. 9 (end) Shear stress τ as a function of fiber concentration F and average volume fraction cl^3 at different shear rates $\dot{\gamma}$ and particle concentrations P=0 and 24%

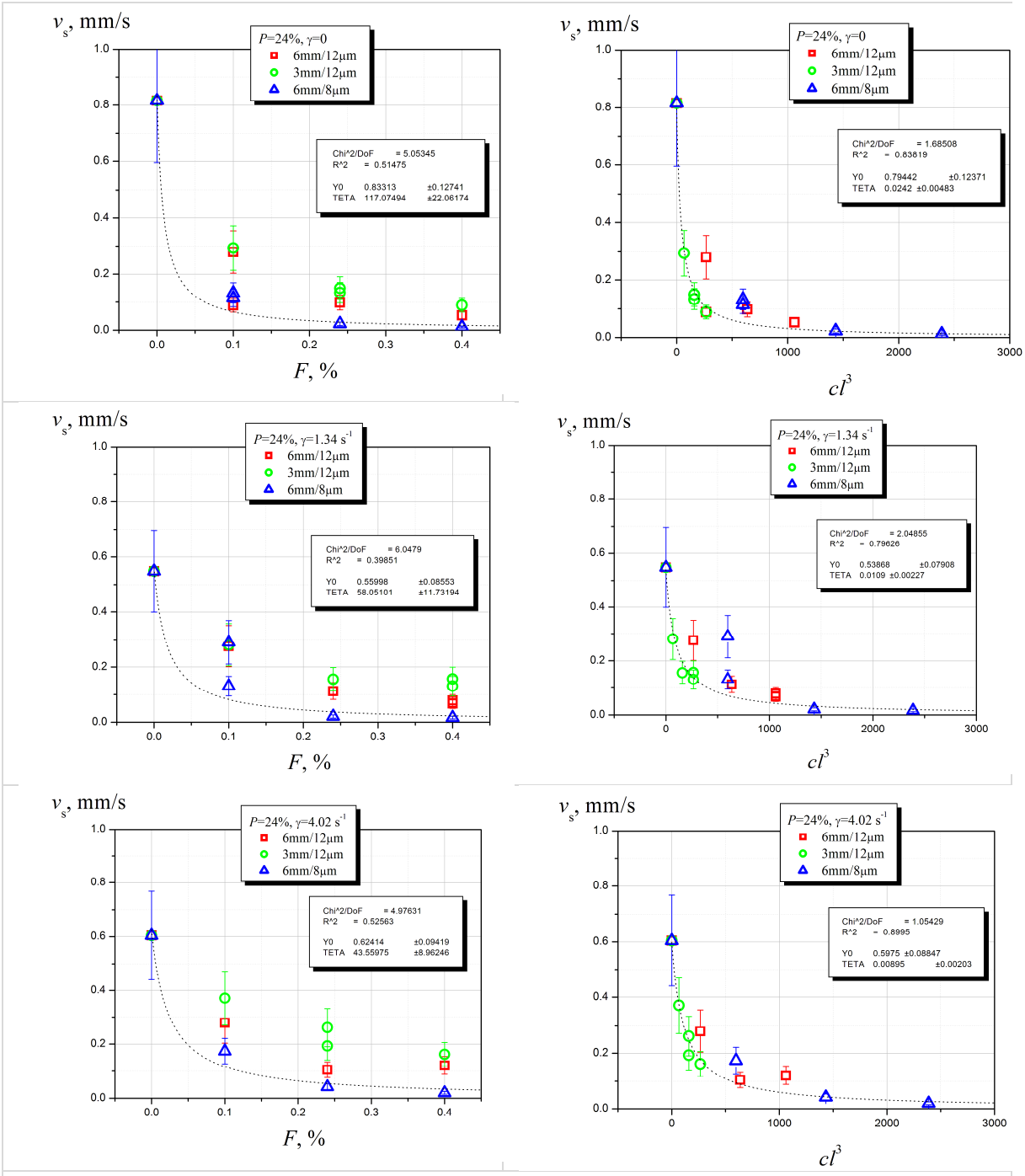

Fig. 10a (beginning)

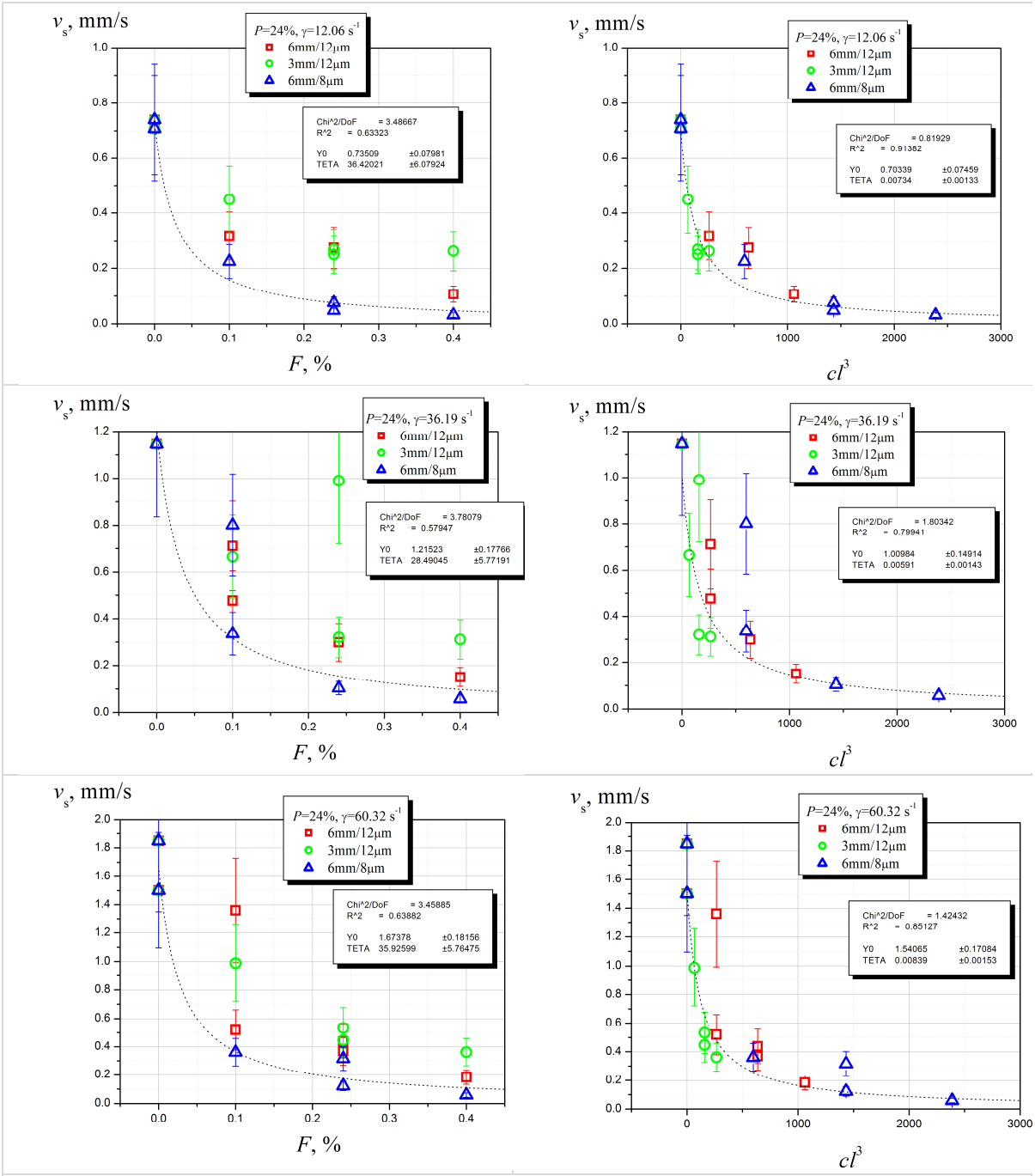

Fig. 10a (continuation)

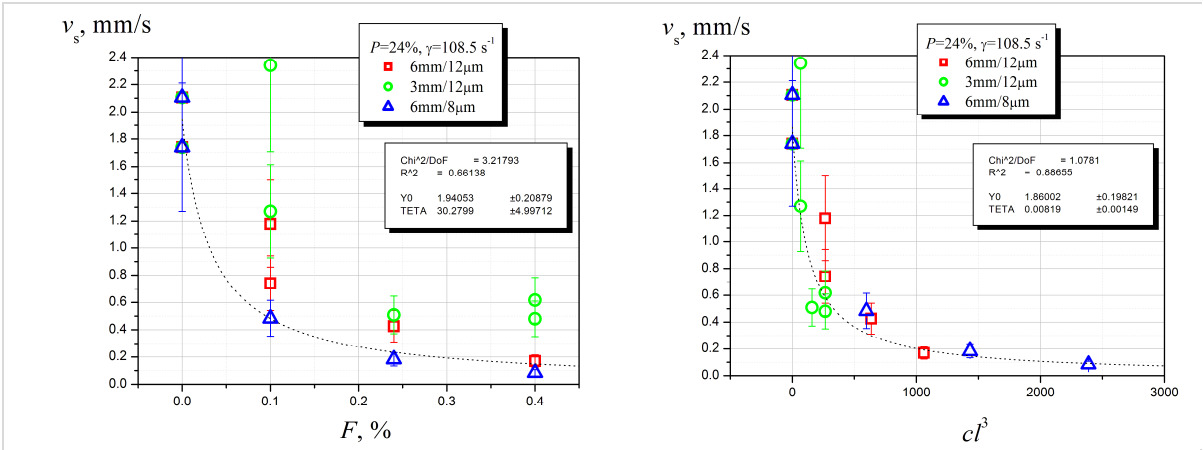

Fig. 10a (end) Sedimentation velocity v_s as a function of fiber concentration F and average volume fraction cl^3. Dotted curves are the fittings with v_s=Y0/(1+TETA*x), where $x=F$ or $x=cl^3$, Y0 and TETA are the fitting parameters. The Instrumental weighting method with error $\sigma=v_s\times\delta v_s$, δv_s~0.2706 (shown in the plot) was used in the fitting procedure

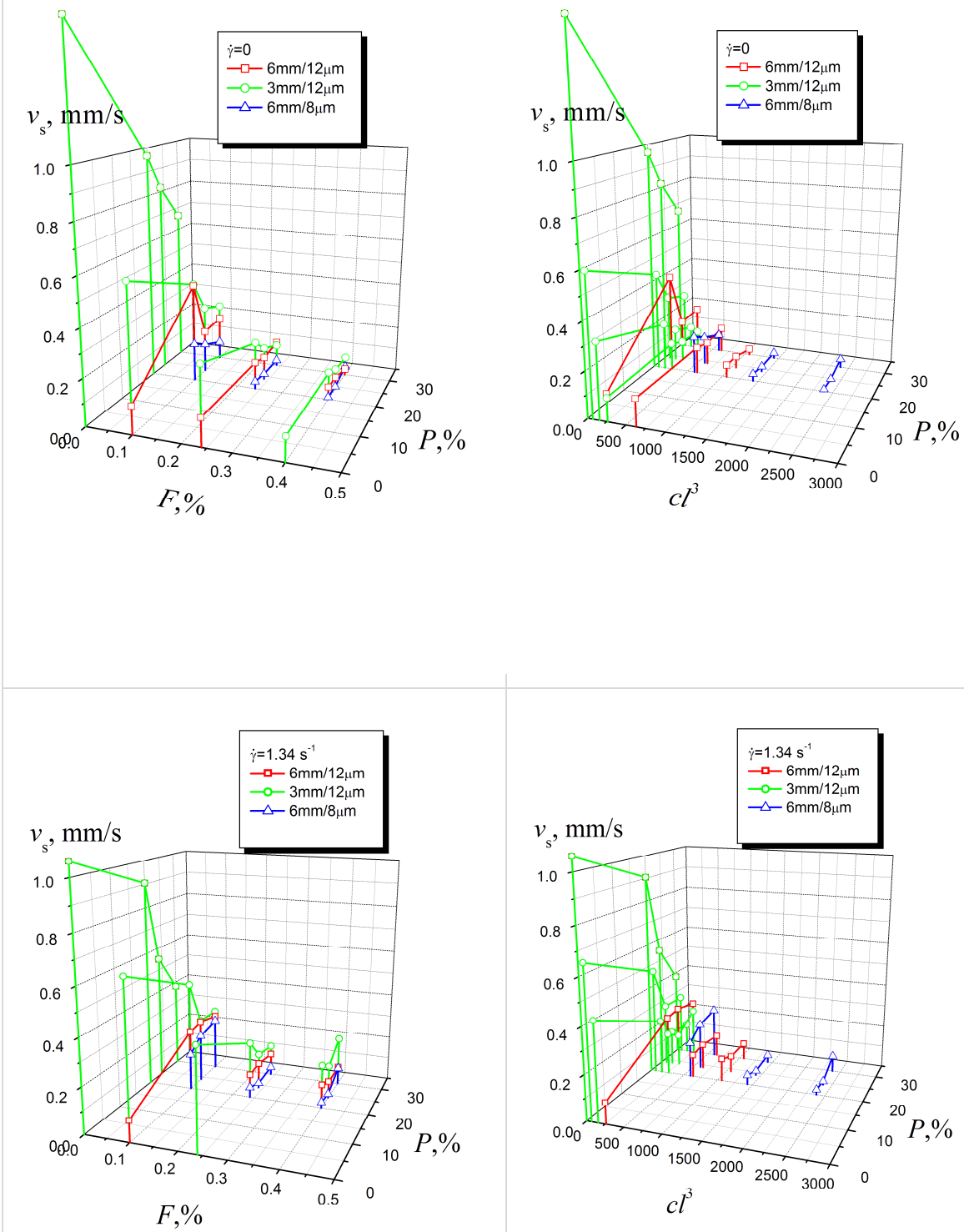

Fig. 10b (beginning)

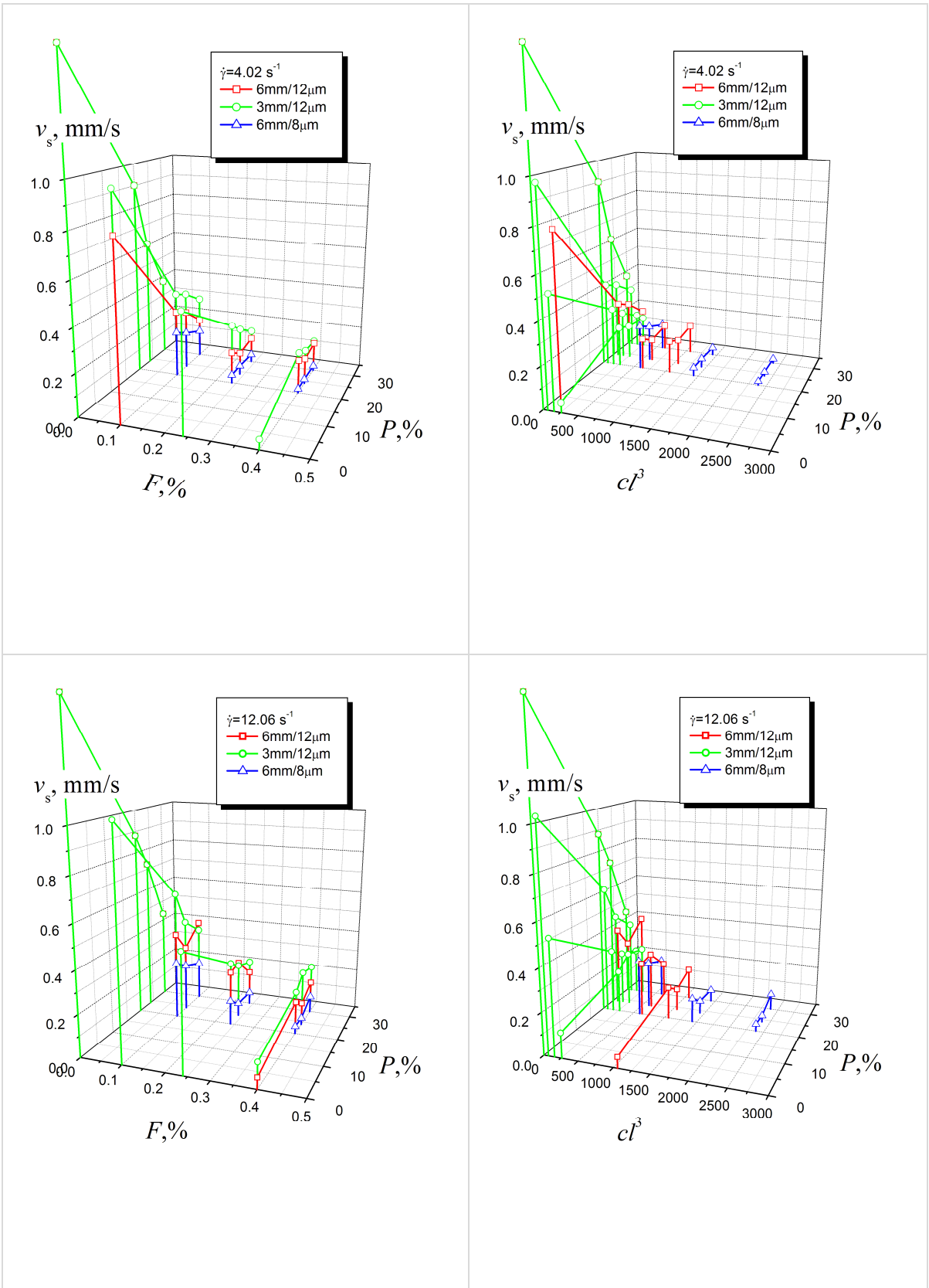

Fig. 10b (continuation)

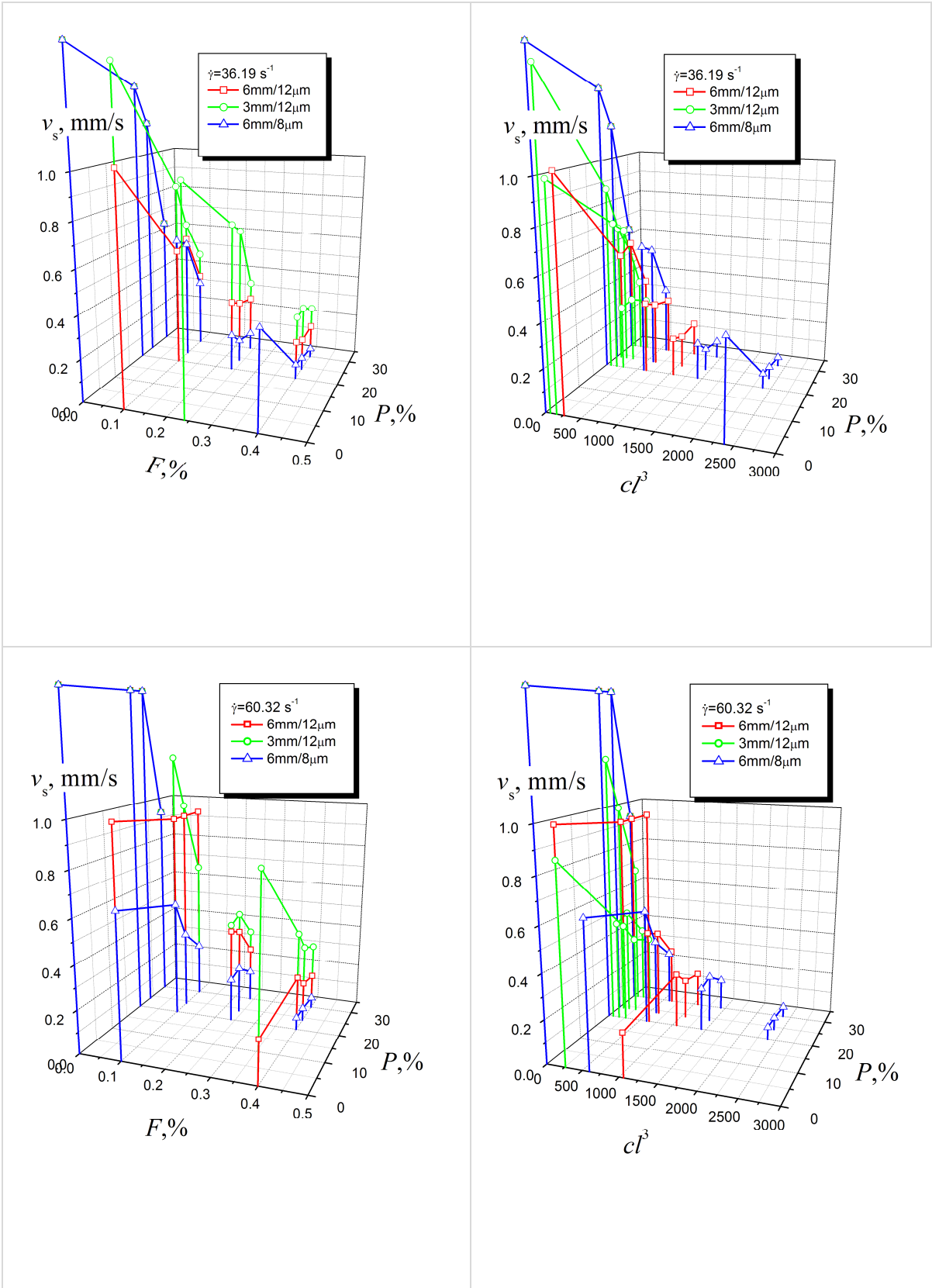

Fig. 10b (continuation)

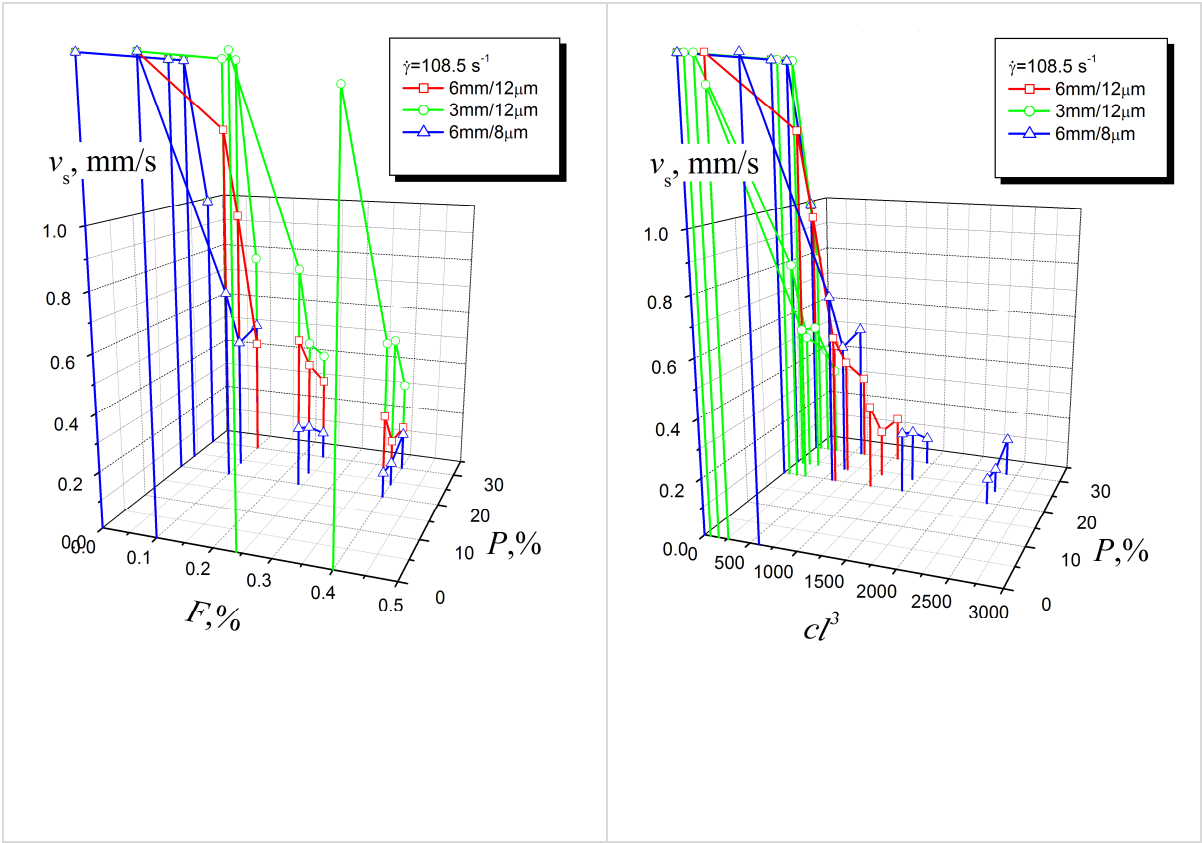

Fig. 10b (end) 3D plot of sedimentation velocity v_s as a function of fiber concentration F and average volume fraction cl^3 for P=0, 20, 24 and 30%

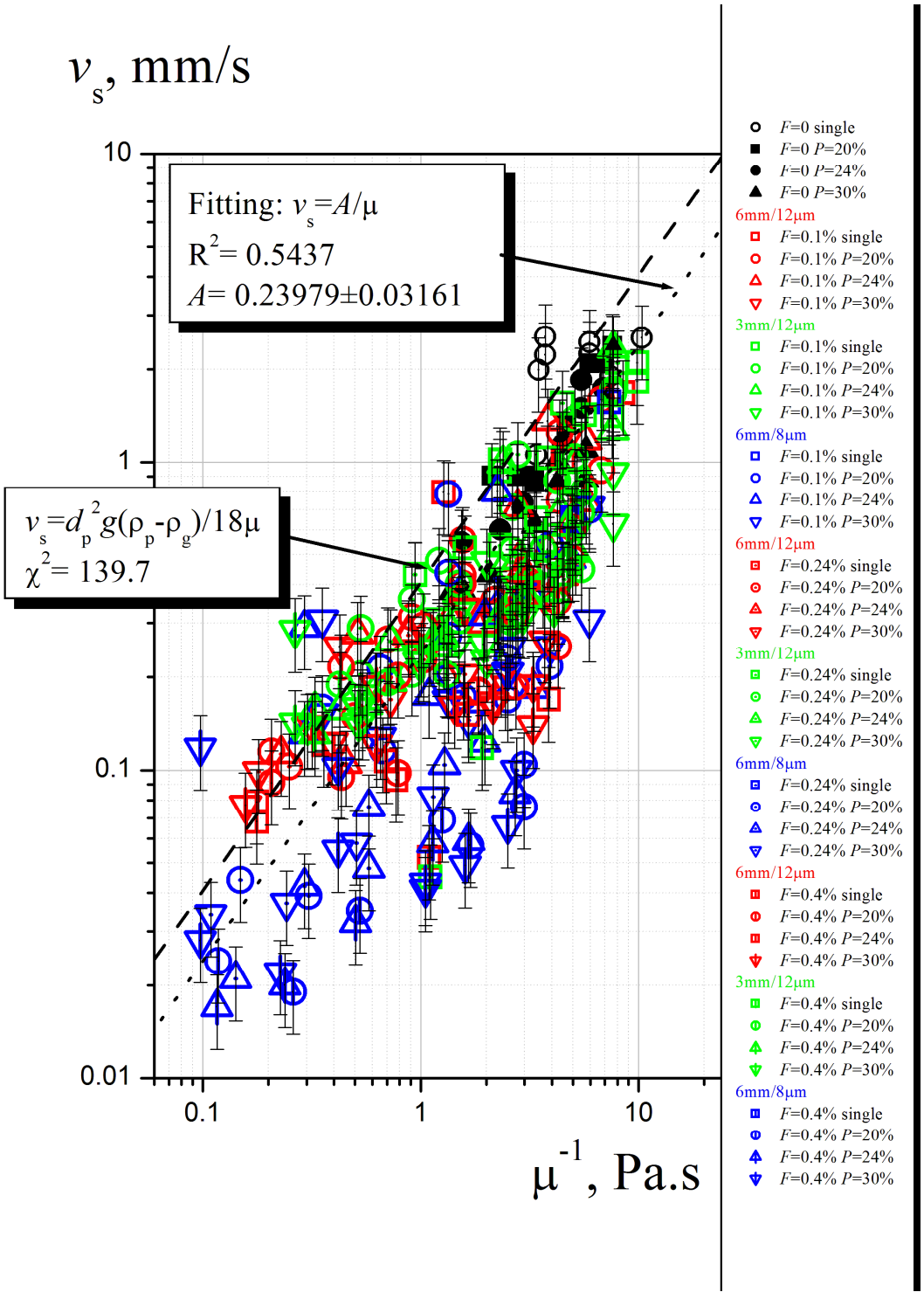

Fig. 11 Relationship between actual viscosity of suspension and particle sedimentation velocity. The concentration of fibers is F=0, 0.1, 0.24, and 0.4%. The concentration of particles P=0 (single particle), 20, 24, and 30%. 283 points are presented

A.V. Bazilevsky
V.A. Kalinichenko
V.A. Plyashkevich
D.V. Badazhkov
A.N. Rozhkov

Sedimentation of particles in shear flows of viscoelastic fluids with fibers

ISBN 978-5-91741-174-3

Подписано к печати 23.06.2016 Заказ № 13-2016 Тираж - 30 экз.

Отпечатано на ризографе Института проблем механики им. А.Ю. Ишлинского РАН
119526 Москва, проспект Вернадского 101, к.1